

1 **Underestimation of Column NO₂ Amounts from the OMI Satellite Compared to Diurnally**
2 **Varying Ground-Based Retrievals from Multiple Pandora Spectrometer Instruments**

3 Jay Herman¹, Nader Abuhassan¹, Jhoon Kim², Jae Kim³, Manvendra Dubey⁴, Marcelo Raponi⁵,
4 Maria Tzortziou⁶

5 **Abstract**

6 Retrievals of Total Column NO₂ (TCNO₂) are compared for 14 sites from the Ozone Measuring
7 Instrument (OMI using OMNO2-NASA v3.1) on the AURA satellite and from multiple ground-
8 based PANDORA spectrometer instruments making direct-sun measurements. While OMI
9 accurately provides the daily global distribution of retrieved TCNO₂, OMI almost always
10 underestimates the local amount TCNO₂ by 50 to 100% in polluted areas, while occasionally the
11 daily OMI value exceeds that measured by PANDORA at very clean sites. Compared to local
12 ground-based or aircraft measurements, OMI cannot resolve spatially variable TCNO₂ pollution
13 within a city or urban areas, which makes it less suitable for air quality assessments related to
14 human health. In addition to systematic underestimates in polluted areas, OMI's selected 13:30
15 equator crossing time polar orbit causes it to miss the frequently much higher values of TCNO₂
16 that occur before or after the OMI overpass time. Six discussed Northern Hemisphere PANDORA
17 sites have multi-year data records (Busan, Seoul, Washington DC, Waterflow New Mexico,
18 Boulder Colorado, and Mauna Loa) and one site in the Southern Hemisphere (Buenos Aires
19 Argentina). The first four of these sites and Buenos Aires frequently have high TCNO₂ (TCNO₂ >
20 0.5 DU). Eight additional sites have shorter term data records in the US and South Korea. One of
21 these is a one-year data record from a highly polluted site at City College in New York City with
22 pollution levels comparable to Seoul, South Korea. OMI estimated air mass factor, surface
23 reflectivity, and the OMI 24x13 km² FOV (field of view) are three factors that can cause OMI to
24 underestimate TCNO₂. Because of the local inhomogeneity of NO_x emissions, the large OMI FOV
25 is the most likely factor for consistent underestimates when comparing OMI TCNO₂ to retrievals
26 from the small PANDORA effective FOV (measured in m²) calculated from the solar diameter of
27 0.5°.

28
29 **Key Words: Nitrogen dioxide, OMI, PAN, PANDORA, ground-based, satellite**

Correspondence email: jay.r.herman@nasa.gov

¹University of Maryland Baltimore County JCET, Maryland

²Department of Atmospheric Sciences, Yonsei National University, South Korea

³Department of Atmospheric Science, Pusan National University, South Korea

⁴Earth Systems Observations, Los Alamos National Laboratory, Los Alamos, NM 87545

⁵Departamento de Investigaciones en Láseres y Aplicaciones (DEILAP), Instituto de Investigaciones Científicas y Técnicas para la Defensa (CITEDEF), Ministerio de Defensa (MINDEF), Buenos Aires, Argentina

⁶City College of New York, New York City, NY

30 Underestimation of Column NO₂ Amounts from the OMI Satellite Compared to Ground-Based 31 Retrievals from Multiple Pandora Spectrometer Instruments

32 1.0 Introduction

33 Retrieval of Total Column NO₂ (TCNO₂) from the Ozone Monitoring Instrument (OMI) has been a
34 scientific success story for the past 14 years. Near total global coverage from the well-calibrated OMI has
35 enabled observation of all the regions where NO₂ is produced and has permitted monitoring of the
36 changes during the 2004 to 2019 period, especially in regions where there is heavy and growing industrial
37 activity (e.g., China and India). TCNO₂ amounts (data used: OMNO2-NASA v3.1) retrieved from OMI over
38 various specified land locations show a strong local underestimate compared to co-located PANDORA
39 Spectrometer Instruments (the abbreviation PAN is used for graph and table labels). The underestimate
40 of OMI TCNO₂ at the overpass time compared to ground-based measurements has previously been
41 reported at a few specific locations (Bechle, 2013; Lamsal et al., 2015; Ialongo et al., 2017; Kollonige, et
42 al., 2018; Goldberg et al., 2018; Herman et al., 2018). The accuracy and precision of PANDORA TCNO₂
43 measurements has been previously discussed (Herman et al., 2009; 2018). For any location, the OMI
44 overpass local standard time consists of the central overpass near the 13:30 hour equator crossing solar
45 time and occasionally a side viewing overpass from adjacent orbits within ±90 minutes of the central
46 overpass time. Independently from instrument calibration and retrieval errors, there are two specific
47 aspects to the underestimation of TCNO₂ pollution levels. Because of OMI's selected polar orbit, it is not
48 possible for the mid-day OMI observations to see the large diurnal variation of TCNO₂ that usually occur
49 after the 13:30 overpass time, and second, because of spatial inhomogeneity the large OMI field of view
50 (FOV) footprint 13 x 24 km² at OMI nadir view tends to average regions of high NO₂ amounts (Nowlan et
51 al., 2016; Judd et al., 2018) with those from lower pollution areas. An analysis by Judd et al., (2019, their
52 Fig. 9) shows the effect of decreasing satellite spatial resolution on improving agreement with PANDORA,
53 with the best agreement occurring with an airborne instrument, GEO-TASO (resolution 3x3 km²) followed
54 by TropOMI (5x5 km²) and then OMI (18x18 km²). Both OMI and TropOMI show an underestimate of
55 TCNO₂ compared to PANDORA.

56 There are other possible systematic retrieval errors with OMI TCNO₂. The largest of these is
57 determining the air mass factor (AMF) needed to convert slant column measurements into vertical column
58 amounts followed by the surface reflectivity Rs (Boersma et al., 2011; Lin et al., 2015; Nowlan et al., 2016;
59 Lorente et al., 2018). Accurately determining the AMF for TCNO₂ requires a-priori knowledge of the NO₂
60 profile shape (Krotkov et al., 2017), which is estimated from coarse resolution model calculations
61 (Boersma et al., 2011), and using the correct Rs. Currently Rs is found using a statistical process of sorting
62 through years of data to find relatively clear-sky scenes for each location (Kleipool, et al., 2008; O'Byrne
63 et al., 2010). Boersma et al., 2004 gave a detailed error analysis for the various components contributing
64 OMI TCNO₂ retrievals resulting an estimated "retrieval precision of 35-60%" in heavily polluted areas
65 dominated by determining the air mass factor. An improved V2.0 DOMINO retrieval (Boersma et al., 2011)
66 algorithm reduced the retrieval errors while increasing the estimated airmass factor, which reduces the
67 retrieved TCNO₂ up to 20% in winter and 10% in summer. The current version of OMNO2-NASA (Krotkov
68 et al., 2017) and v2.0 DOMINO (Boersma et al., 2011) are generally in good agreement (Marchenko et al.,

69 2015; Zara et al., 2018). However, the OMNO2-NASA TCNO₂ retrievals are 10 to 15% lower than the v2.0
70 DOMINO retrievals and with Quality Assurance for Essential Climate Variables (QA4ECV) retrievals. A
71 subsequent detailed analysis of surface reflectivity (Vasilkov et al., 2017) shows that retrieval of TCNO₂ in
72 highly polluted areas (e.g., some areas in China) can increase by 50% with the use of geometry-dependent
73 reflectivities, but only increase about 5% in less polluted areas. For PANDORA, calculation of the solar
74 viewing AMF is a simple geometric problem (AMF is approximately proportional to the cosecant of the
75 solar zenith angle SZA) and is independent of R_s (Herman et al., 2009). For a highly polluted region with
76 TCNO₂ = 5.34x10¹⁶ molecules/cm² or 2 DU, the PANDORA error is expected to be less than 2 ± 0.05 DU
77 (±2.5%) with the largest uncertainty coming from an assumed nominal amount of stratospheric TCNO₂ =
78 0.1 DU.

79 Accurate satellite TCNO₂ retrievals (and for other trace gases) are important in the estimate of
80 the effect of polluted air containing NO₂ on human health (Kim and Song, 2017 and references therein),
81 especially from the viewpoint of NO₂ as a respiratory irritant and precursor to cancer (Choudhari et al.,
82 2013). Since NO₂ is largely produced by combustion, satellite observations of NO₂ serve as a proxy for
83 changing industrial activity. Another important application requiring accurate measurements of the
84 amount of TCNO₂ and its diurnal variation is atmospheric NO₂ contribution to nitrification of coastal
85 waters (Tzortziou et al., 2018).

86 We show that the use of OMI TCNO₂ for estimating local air quality and coastal nitrification on a
87 global basis is misleading for most polluted locations, and especially on days when the morning or
88 afternoon amounts are higher than those occurring at the OMI overpass time near 13:30 hours standard
89 time. OMI TCNO₂ data are extremely useful for estimating regional pollution amounts and for assessing
90 long-term changes in these amounts. Modelling studies (Lamsal et al., 2017 Fig. 1) based on the Global
91 Modelling Initiative model (Strahan et al., 2007) simulating TCNO₂ diurnal variation over Maryland USA
92 (37-40°N, 74-79°W) shows a late afternoon peak and shows that the stratospheric component does not
93 substantially contribute to this peak. Boersma et al. (2016) show that sampling strategy can cause
94 systematic errors between OMI TCNO₂ and model TCNO₂ with satellite results being up to 20% lower than
95 models. Duncan et al., (2014) reviews the applicability of satellite TCNO₂ data to represent air quality and
96 notes that TCNO₂ correlates well with surface levels of NO₂ in industrial regions and states that the portion
97 of TCNO₂ in the boundary layer could be over 75% of the total vertical column depending on NO₂ altitude
98 profile shape.

99 This paper presents 14 different site comparisons between retrieved OMI TCNO₂ overpass values
100 that are co-located with PANDORA TCNO₂ amounts from various locations in the world. Six of the
101 comparisons are where PANDORAs have long-term data (1-year or longer) records. The comparisons are
102 done using 80 second cadence data matched to the OMI overpass times averaged over ±6 minutes and
103 with monthly running averages calculated using Lowess(f) (Locally Weighted least squares fit to a fraction
104 f of the data points, (Cleveland, 1981) of OMI-PANDORA time matched TCNO₂. OMI overpass data,
105 <https://avdc.gsfc.nasa.gov/index.php?site=666843934&id=13>, are filtered for the row anomaly and
106 cloudy pixels. The selection of a ±6-minute window represents 720 seconds or 9 PANDORA
107 measurements averaged together around the OMI overpass time to reduce the effect of outlier points.
108 The specific value of ±6 minutes is arbitrary but increases the already high effective signal to noise ratio

109 by a factor of 3. PANDORA data are filtered for significant cloud cover by examining the effective variance
110 in sub-interval (20 seconds) measurements. Each PANDORA listed measurement is the average of up to
111 4000 (clear sky) individual measurement made over 20 seconds.

112

113 This paper gives a discussion and presentation of data on the effect of diurnal variation that are
114 always missed at the local OMI mid-day overpass times. We show that OMI TCNO₂ values are also
115 systematically lower than PANDORA values at sites with significant pollution (TCNO₂ > 0.3 DU). We present
116 a unique view of a year of fully time resolved diurnal variation of TCNO₂ at two sites, Washington DC and
117 New York City, which are similar to other polluted locations.

118

119 **2.0 Brief Instrument Descriptions**

120 For the purposes of TCNO₂ retrievals, both OMI and PANDORA are spectrometer-based
121 instruments using nearly the same spectral range and similar spectral resolution (about 0.5 nm). Both use
122 spectral fitting retrieval algorithms that differ (Boersma et al. 2011; Herman et al., 2009) because of the
123 differences between direct-sun viewing retrievals (PANDORA) and above the atmosphere downward
124 viewing retrievals (OMI). The biggest difference is with the respective fields of view, 13 x 24 km² at OMI
125 nadir view and larger off-nadir FOV compared to the much smaller PANDORA FOV (1.2^o) measured in m²
126 with the precise value depending on the NO₂ profile shape and the solar zenith angle. For example, if most
127 of the TCNO₂ is located below 2 km, then the PANDORA FOV is approximately given by
128 $(1.2\pi/180)(2/\cos(\text{SZA}))$, which for SZA = 45^o is about 59x59 m². If the solar disk (0.5^o) is used as the limiting
129 factor, then the effective FOV is smaller (25x25 m²).

130 **2.1 OMI**

131 OMI is an east-west side (2600 km) and nadir viewing polar orbiting imaging spectrometer that
132 measures the earth's backscattered and reflected radiation in the range 270 to 500 nm with a spectral
133 resolution of 0.5 nm. The polar orbiting side viewing capabilities produce a pole to pole swath that is about
134 2600 km wide displaced in longitude every 90 minutes by the earth's rotation to provide coverage of
135 nearly the entire sunlit Earth once per day at a 13:30 solar hour equator crossing time with spatial gaps at
136 low latitudes. OMI provides full global coverage every 2 to 3 days. Additional gaps are caused by a problem
137 with the OMI CCD, "row anomaly" (Torres et al., 2018) that effectively reduces the number of near-nadir
138 overpass views. A detailed OMI instrument description is given in Levelt et al. (2006). TCNO₂ is determined
139 in the visible spectral range from 405 to 465 nm where the NO₂ absorption spectrum has the maximum
140 spectral structure and where there is little interference from other trace gas species (there is a weak water
141 feature in this range). OMI TCNO₂ overpass data are available for many ground sites (currently 719) from
142 the following NASA website. <https://avdc.gsfc.nasa.gov/index.php?site=666843934&id=13> (valid as of 16
143 July 2019).

144

145 **2.2 PANDORA**

146

147 PANDORA is a sun-viewing instrument for SZA < 80^o that obtains about 4000 spectra for clear-sky
148 views of the sun in 20 seconds for each of two ranges UV (290 – 380 nm using a UV340 bandpass filter)

149 and visible plus UV (280 – 525 nm using no filter). The overall measurement time is about 80 seconds
150 including a 20 second dark-current measurements between each spectral measurement throughout the
151 day. About 4000 clear-sky spectra for the UV and visible portions are separately averaged together to
152 achieve very high signal to noise ratios (SNR). The UV340 filter for UV portion of the spectra reduces stray
153 light effects from the visible wavelength range. A detailed description of PANDORA and its SNR is given
154 in Herman et al., (2009; 2015). The effect of moderate cloud cover (reduction of observed signal by a
155 factor of 8) in the PANDORA FOV on TCNO₂ retrievals is small (Herman et al., 2018). Cloud cover also
156 reduces the number of measurements possible in 20 seconds, which potentially increases the noise level.
157 PANDORA is driven by a highly accurate sun tracker that points an optical head at the sun and transmits
158 the received light to an Avantes 2048 x 32 pixel CCD spectrometer (AvaSpec-ULS2048 from 280 – 525 nm
159 with 0.6 nm resolution) through a 50 micron diameter fiber optic cable. The estimated TCNO₂ error is
160 approximately 0.05 DU (1 DU = 2.69 x 10¹⁶ molecules cm⁻²) out of a typical value of 0.3 DU in relatively
161 clean areas and over 3 DU in highly polluted areas. PANDORA data are available for 250 sites. Some sites
162 have multi-year data sets, but many of these sites are short-term campaign sites.
163 https://avdc.gsfc.nasa.gov/pub/DSCOVER/Pandora/DATA_01/. (valid as of 16 July 2019).
164

165 **3.0 Overpass Comparisons and Diurnal Variation of TCNO₂**

166

167 The contribution of NO₂ to air quality at the Earth's surface is usually a proportional function of
168 TCNO₂ that varies with the time of day and with the altitude profile shape (Lamsal et al., 2013; Bechle et
169 al., 2013). Most of the NO₂ amount is usually located between 0 and 3 km altitude with a small amount of
170 about 0.1±0.05 DU (Dirksen et al. 2011) in the upper troposphere and stratosphere. Because of the
171 relatively short chemical lifetime, 3-4 hours (Liu et al., 2016), in the lower atmosphere, most of the NO₂ is
172 located near (0 to 20 km) its sources (industrial activity, power generation, and automobile traffic). At
173 higher altitudes or in the winter months, the life time of NO₂ is longer permitting transport over larger
174 distances from its sources.

175
176 During the South Korean campaign (KORUS-AQ) in the spring of 2016 the diurnal variations of
177 TCNO₂ vs days of the year DOY were determined for 6 sites (Herman et al., 2018), one of which is
178 reproduced here (Fig. 1) for the city of Busan showing relatively low values of TCNO₂ in the morning (0.5
179 DU), moderately high values during the middle of the day (1.3 DU), and very high values on some of the
180 afternoons (2 to 3 DU). Of these data, OMI only observes midday values near the 13:30 time marked on
181 the Local_Time axis of Fig.1 thereby missing very high values (2 to 3 DU) that frequently occur later in the
182 afternoon coinciding with times when people are outdoors returning from work.

183
184 In addition to not being designed to observe the TCNO₂ diurnal variation, the OMI values are
185 about half those observed by PANDORA (Fig. 2) at the OMI overpass time, so that using OMI values to
186 estimate NO₂ pollution seriously underestimates the air quality problem even at midday. The shaded area
187 in Fig.2 corresponds to the period covered in the KORUS-AQ campaign 7 April to 11 June 2016 shown in
188 Fig. 1. An extended time series for Busan location is shown in Fig. 3.

189

190 Because of the different effective NO₂ FOV of PANDORA (measured in m²) while tracking the
191 moving sun position located in the heart of Busan (FOV distance $d < 5$ km for an SZA $< 70^\circ$ used for
192 TCNO₂ retrievals), both the daily (Fig. 3, left panel) and PANDORA monthly average variation (Fig. 3, right
193 panel), obtained at the OMI overpass time, differs from the variation in the OMI TCNO₂ caused by the
194 much larger OMI FOV (13 x 24 km² at OMI nadir view) retrieval. Because of this, the OMI time series has
195 low correlation ($r^2 = 0.1$) with the PANDORA time series.

196
197 The extended OMI vs PANDORA time series from 2012 – 2017 for Busan (Fig. 3) shows the same
198 magnitude of differences seen during the KORUS-AQ period. A similar OMI vs PANDORA plot for total
199 column ozone TCO₃ (Appendix Fig A1) shows good agreement between PANDORA and OMI indicating that
200 the PANDORA instrument was operating and tracking the sun properly. Because the spatial variability of
201 TCO₃, which is mostly in the stratosphere, is much less than for TCNO₂, the effect of different FOV's is
202 minimized for ozone.

203
204 The same type of differences, TCNO₂(PAN) > TCNO₂(OMI), are seen at a wide variety of sites (e.g.,
205 see Fig.4 and Fig. 5) for Northern Hemisphere sites and one site in the Southern Hemisphere where
206 PANDORA has an extended time series. Comparing extended Busan multi-year time series, some broad-
207 scale correlation can be seen with peaks in February 2013, January 2014, and in 2016. The OMI data from
208 Busan are different than data from many sites, since Busan is located very near the ocean causing a portion
209 of the OMI FOV to be over the relatively unpolluted ocean areas, whereas PANDORA is located inland
210 (Pusan University) in an area of dense automobile traffic and quite near mountains capable of trapping
211 air.

212
213 Figures 4 and 5 show a variety of different sites, ranging from the Mauna Loa Observatory location
214 at 3.4 km (11,161 feet) on a relatively clean Hawaiian Island surrounded by ocean to a polluted landlocked
215 semi-arid site at Waterflow, New Mexico near a power plant. All the sites considered show a significant
216 underestimate of OMI TCNO₂. A summary of the monthly average underestimates is given in Tables 1 and
217 2. For some sites there is evident correlation between the two offset measurements. For example, the
218 PANDORA at NASA Headquarters in Washington DC tracks the OMI measurement quite well on a monthly
219 average basis with a correlation coefficient of $r^2(\text{mn}) = 0.7$ even though the daily correlation is low ($r^2(\text{dy})$
220 = 0.17). Other sites have only short periods of correlation and overall weak correlation (Table 1 showing
221 daily, dy and monthly, mn, correlation coefficients for the graphs in Figures 4 and 5)

222
223 TCNO₂(PAN) comparisons with TCNO₂(OMI) from Mauna Loa Observatory MLO (Fig. 4) are not
224 those that might be expected, since the PANDORA observations are in an area where there are almost no
225 automobile emissions and certainly no power plants, yet PAN > OMI and TCNO₂(PAN) values are large
226 enough so that the pollution values (0.18 DU) are well above the stratospheric values (approximately 0.1
227 DU). OMI, which mainly measures values over the clean ocean, has an average value of about 0.1 DU (see
228 appendix Fig. A2). Since there are no emission or combustion sources of NO₂ at high altitudes near MLO
229 at 3.4 km, the PANDORA values suggest upward airflow from the near sea level circumferential ring road,
230 Keahole oil power plant, and resort areas. The Mauna Loa TCNO₂ values do not show any correlation with
231 the recent increased volcanic activity at Mt. Kilauea after 2016. A graph showing the mid-day values of

232 TCNO₂ at MLO is given in the appendix. Recently, the original Mauna Loa PANDORA has been replaced.
 233 The new instrument's calibration will be reviewed before being added to the time series as part of a
 234 general data quality assurance program that is starting with the most recently deployed or upgraded
 235 PANDORA instruments at about 100 locations.

Table 1 Values of TCNO₂ for PANDORA and OMI from monthly averages in Figs. 4 and 5

Name	Location (Lat, Lon)	PAN (DU)	OMI (DU)	r ² (dy, mn)
Mauna Loa Hawaii	19.536°, -155.5762°	0.16	0.11	0.01, 0.30
NASA HQ Washington DC	38.882°, -77.01°	0.34	0.25	0.17, 0.70
Waterflow New Mexico ¹	36.797°, -108.48°	0.32	0.18	0.13, 0.52
Seoul South Korea	37.5644°, 126.934°	1.2	0.58	0.11, 0.06
Busan South Korea	35.2353°, 129.0825°	0.68	0.32	0.09, 0.10
Boulder Colorado	39.9909°, -105.2607°	0.27	0.17	0.04, 0.09
Buenos Aires Argentina	-34.5554°, -58.5062°	0.50	0.26	0.16, 0.08
Average		0.49	0.27	

236

Table 2 Average values of TCNO₂ for PANDORA and OMI for additional sites

Name	Location (Lat, Lon)	PAN (DU)	OMI (DU)
Essex Maryland	39.31083°, -76.47444°	0.30	0.28
Baltimore Maryland	39.29149°, -76.59646°	0.45	0.27
Fresno California	36.7854°, -119.7731°	0.42	0.17
Denver La Casa Colorado	39.778°, -105.006°	0.68	0.19
GIST ²	35.226°, 126.843°	0.42	0.20
HUFS ³	37.338°, 127.265°	0.61	0.51
City College New York City	40.8153°, -73.9505°	0.60	0.40
Average		0.50	0.29

¹Waterflow, NM is listed for OMI data as Four Corners, NM, a nearby landmark

²Gwangju Institute of Science and Technology S. Korea

³Hankuk University Foreign Studies South Korea

237

238 An interesting inland site is near the very small town of Waterflow, New Mexico (Figs. 4 and 6),
 239 where two power plants located near the PANDORA site ceased operation on December 30, 2013
 240 (Lindenmaier et al., 2014). According to a quote from AZCentral Newspaper (Tuesday 31 December 2013)
 241 "Three coal-fired generators that opened in the 1960s near Farmington, N.M., closed Monday as part of
 242 a \$182 million plan for Arizona Public Service Co. to meet environmental regulations, the utility reported".
 243 The TCNO₂ data suggests that the actual shutdown occurred near October 15, 2013. After the shutdown,
 244 air quality improved in the area with TCNO₂ decreasing from 0.4 DU to 0.28 DU. The remaining more
 245 efficient generators continued to produce smaller NO₂ emissions. These were shut down at the end of
 246 2016 with little additional observed change in TCNO₂, since these boilers used NO₂ scrubbers (Dubey at
 247 al., 2018 in preparation). A nearby highway (Route 64) about 2 km from the PANDORA site has little
 248 automobile traffic. An example of the diurnal behavior of TCNO₂ at Waterflow, New Mexico on 6 June
 249 2012 is shown in Fig. 6 to illustrate the behavior of PANDORA TCNO₂ retrievals at a wide range of SZA. The

250 terrain surrounding the Waterflow Pandora site is flat with no obstructions (buildings) permitting
251 observations to very high SZA. Almost every day the power plant briefly puts out very high emissions of
252 NO₂ as part of its daily boiler cleaning cycle. This can be seen in the very high peak value of TCNO₂ of 3.4
253 DU compared to the nominal value of 0.5 DU occurring for most of the day. The value from the FOV
254 averaged OMI retrieval at 21:01 GMT (14:01 local standard time) is about 0.2 DU compared to the
255 PANDORA value of about 0.5DU. Figure 6 also illustrates TCNO₂ diurnal behavior at two other sites, NASA
256 HQ in Washington, DC and at City College of New York and compares the values to the OMI retrieved
257 TCNO₂.

258
259 Both Figs. 6 and 2A show the PANDORA TCNO₂ retrieval with the values of the SZA plotted on the
260 same graph showing that the direct-sun retrievals are good out to SZA = 70°. Depending on atmospheric
261 conditions, retrievals using BEER's law absorption attenuation and spectral fitting for SZA > 75° begin to
262 yield non-physical values (TCNO₂ too small). During mid-day measurements, the signal to noise ratio is
263 very high since over 4000 clear-sky measurements are averaged together to produce one data point every
264 20 seconds. Even with aerosol loading (no spectral features) or moderate cloud cover blocking the sun,
265 the retrievals are still accurate (Herman et al., 2018).

266
267 Table 2 contains a summary of some sites that were part of short-term Discover-AQ campaigns in
268 Maryland, Texas, California, and Colorado, two longer-term sites in South Korea, and one in New York
269 City. Essex, Maryland is located on the Chesapeake Bay 10 km east of the center of Baltimore. The site is
270 relatively clean (PAN = 0.3 DU) compared to the center of Baltimore (PAN = 0.45 DU), while OMI measures
271 about the same amounts for both sites (0.28 and 0.27 DU) because the OMI FOV is larger than the distance
272 between the two sites. The Houston Texas site contains 7 months of data from January to July 2013 with
273 widespread NO₂ pollution permitting PANDORA and OMI to measure the same average values even
274 though PANDORA observes episodes on many days when TCNO₂ exceeds 1.5 DU for short periods at times
275 not observed by OMI. Observations in the small city of Fresno, California were during January when
276 agricultural sources of NO₂ were at a minimum (Almaraz, 2018), but automobile traffic in the center of
277 Fresno was significant. In this situation, PANDORA recorded the effect of automobile traffic while OMI
278 averaged the city of Fresno and surrounding fallow agricultural areas. The Denver La Casa location is in
279 the center of the city in an area with high amounts of local automobile traffic and near the Cherokee
280 power generating plant. The result is a high level of average pollution (0.42 DU) while OMI measures both
281 the city center and the surrounding relatively clean plains areas. The HUFs South Korean site is southeast
282 of Seoul in a fairly isolated valley. However, Seoul and its surrounding areas are a widespread transported
283 source of pollution so that both PANDORA and OMI measure elevated TCNO₂ amounts. In contrast, the
284 PANDORA GIST site is on the outskirts of a small city in southwestern South Korea with significant traffic.
285 The result is significant amounts of localized TCNO₂ (PANDORA = 0.42) surrounded by areas that produce
286 little NO₂ leading to OMI observing a very clean 0.2 DU. The average of sites in the two tables are similar
287 leading to ratios of PAN/OMI of 1.8 and 1.7, respectively. The estimated 50% increase in OMI retrievals of
288 TCNO₂ from using the geometry-dependent reflectivity (Vasilkov, 2017) for the most polluted sites will
289 narrow the disagreement with PANDORA. For example, OMI Seoul TCNO₂ may become 0.87 DU
290 (PANDORA = 1.2 DU) and Buenos Aires 0.39 DU (PANDORA = 0.5 DU) still underestimating the amount of
291 NO₂ pollution and missing the significant diurnal variation.

292 For the six sites shown, the average OMI underestimate of TCNO₂ is approximately a factor of 1.8
293 at the overpass time on a monthly average basis with occasional spikes that exceed this amount. The bias
294 values range from 1.1 to 3.6, with higher biases tending to be associated with higher TCNO₂ values. The
295 factor of 1.8 underestimate ignores the frequent large values of TCNO₂ at other times during the day (Fig.
296 7). In addition, averaging TCNO₂(PAN) over each entire day yields average values for the whole period that
297 are 10 to 20% higher than just averaging over midday values that matched the OMI overpass time. Aside
298 from the absolute magnitude, the short-term variations (over several months) are similar for both OMI
299 and PANDORA although mostly not correlated. If correlation coefficients r^2 are generated from linear fits
300 to scatter plots of TCNO₂ from OMI vs PANDORA, the correlation is mostly poor (Examples, r^2 =: Seoul
301 0.06, Mauna Loa 0.3 NASA HQ 0.7, see Figs. 4 and 5). Additional sites with shorter PANDORA time series
302 of TCNO₂ show similar behavior.

303 Duncan et al. (2016) estimated trends from OMI TCNO₂ time series and found that the Seoul
304 metropolitan area had a decrease of -1.5 ± 1.3 %/Year (2005 – 2014) consistent with OMI estimated
305 change of $-1.4 \pm 1\%$ /year (2012 -2018) in this paper. However, for the small area near Yonsei University,
306 the decrease estimated from PANDORA is -5.8 ± 0.75 %/Year. Park (2019) estimates that metropolitan
307 Seoul has decreased in population even as surrounding areas have increased population.

308 The average percent differences between OMI and PANDORA shown in Fig. 7 are relatively
309 constant over time for each site with small changes over each multi-year observation period. The
310 differences between OMI and PANDORA are provided by forming the percent differences of the daily
311 TCNO₂ values (Fig. 7) in the form $100(\text{OMI} - \text{PAN})/\text{PAN}$. Also shown are the average percent differences
312 and the linear fit slopes in percent change per year of the percent differences over the multi-year period.
313 For example, the Boulder percent difference goes from -31% to -23% over 4 years. Of the six sites in shown
314 in Fig. 7, two have statistically significant slopes, Seoul South Korea 2.1 ± 0.5 %/Year and NASA
315 Headquarters in Washington DC 3.4 ± 0.9 %/Year at the 2σ level suggesting a significant area average
316 increase in pollution compared to PANDORA's local values.

317 For some sites (see Fig. 7), PANDORA and OMI trends are the same within statistical uncertainty
318 (Waterflow, NM, Buenos Aires, and Mauna Loa) while the other 3 sites show significantly different trends
319 (Boulder, NASA HQ, and Seoul).

320 The results for Busan (from Fig. 3) show a least squares average for the percent difference of -48
321 $\pm 0.8\%$ for the 2012 – 2018 period with a slope of $6.8 \pm 1\%$ /Year. There is a decrease in the percent
322 difference after October 2015 (Fig. 3) that is mainly from PANDORA seeing less TCNO₂ than during the
323 2012 – 2014 period. There is a gap in the Busan time series from July 2014 until April 2015 when the
324 original PANDORA was replaced with a new instrument. The calibrations of both PANDORAS appear to be
325 correct. Because of the break in the time series it is not clear whether there was a change in local
326 conditions around Pusan University compared to the wide area observed by OMI.

327

328

3.1 Diurnal Variation of TCNO₂ Compared to OMI Retrievals

Figure 8 shows details of the daily diurnal variation of TCNO₂ on the roof of NASA Headquarters Washington, DC adjacent to a major cross-town highway (I695) for every day during each month of 2015 for local time vs DOY. The midday observing local standard time for OMI is marked for each graph. Displaying an entire year of daily (2-minute time resolution) PANDORA data shows that the high values of TCNO₂ are a frequent occurrence but do not occur every day.

The amount of TCNO₂ is mostly from the adjacent highway and the surrounding urban area with heavy traffic. The relatively moderate TCNO₂ values (0.4 to 0.8 DU) are probably a testament to the effectiveness of catalytic converters mandatory on all US automobiles in such a high traffic area (Bishop and Steadman, 2015). The same data are plotted in Fig. 6 for 8 June 2017 showing that OMI reasonably matched the values seen by PANDORA at 14:00 and 15:00 but was not available to observe high values that occurred in the morning.

Figure 9 contains the daily TCNO₂ diurnal variability vs DOY for each month measured by a PANDORA from the roof of a building on the CCNY (City College of New York) campus in the middle of Manhattan in New York City (NYC). From the values shown, the pollution levels are quite high, rivaling the pollution levels in Seoul, South Korea (see Fig. 5). OMI at its mid-day overpass time would detect some of the high-level pollution events, but miss many others occurring mostly in the afternoon. There are a significant number of days in all the months where the TCNO₂ levels appear to be low (e.g., blue color in July and October), but the blue color still represents significant pollution levels (TCNO₂(PAN) > 0.5 DU) that are small only compared to the peak values during the month (TCNO₂(PAN) > 1 DU). The highest amount of TCNO₂ recorded during 2018 was about 5DU on 13 July 2018 from 11:20 and 12:30 EST (a time with very light winds (1 km/hr) and moderate temperature (25°C). There were many smaller peaks between 2 and 3 DU throughout the year. Extreme cases of high NO₂ amounts are frequently associated with the local meteorology indications of stagnant air (Harkey et al., 2015), The same data are shown in Fig. 6 for two days, 7 May 2018 and 7 June 2018 showing the comparison with OMI and the occurrence of much higher values of TCNO₂ in the morning and afternoon.

For both Washington DC (Fig. 8) and New York City (Fig. 9) there is strong day-to-day and month to month variability that depends on the local meteorological conditions (Seo et al., 2018; Zeng et al., 2015) and the amount of automobile traffic in the area (Andersen et al., 2011; Amin et al., 2017). High TCNO₂ events occur most often in the afternoon such that the OMI overpass near 13:30 would miss most high TCNO₂ events. Poor air quality affecting respiratory health would be improperly characterized by both the OMI average values being too low (Fig. 4) and by missing the extreme pollution events that occur frequently in the late afternoon. The high value of TCNO₂ that occurred on 5 August (2.2 DU) at 07:45 EST for Washington DC is not a retrieval error (SZA less than 70°), but is a one-time anomaly in 2015 compared to more usual high values of 1.5 DU with an occasional spike to 2 DU. It should be noted that TCNO₂ does not accurately represent the NO₂ concentration at the surface, since it is mostly a measure of the amount in the lower 2 km. However, it is roughly proportional to the surface measurements close to the pollution sources (Bechle et al., 2013; Knepp et al., 2014) with the exact proportionality dependent on the profile shape near the ground.

368 Similar daily diurnal variation graphs of TCNO₂ (Figs. 8 and 9) could be shown for each site.
369 However, the basic idea is the same for each site. OMI underestimates the amount of TCNO₂ because of
370 its large FOV and misses most of the peak events at other times of the day. For some sites, such as Busan
371 and Seoul, the peak values can reach 3 DU and above late in the afternoon, which are never seen by OMI
372 (Herman et al., 2018).

373 Figure 10 for CCNY is similar to the graphs in Figs. 4 – 6 showing the relative behavior between
374 PANDORA and OMI but including only OMI pixels that are at a distance $D < 30$ km from CCNY. The results
375 are almost identical to those when $D < 80$ km. There is a period in March 2018 when OMI TCNO₂ slightly
376 exceeded that measured by PANDORA. OMI with its large FOV may be seeing part of the chemically driven
377 seasonal variation, while PANDORA is seeing a nearly constant source driven amount mostly from
378 automobile traffic. For most days during 2018, $PAN(TCNO_2) > OMI(TCNO_2)$ with the average value for PAN
379 = 0.65 DU and for OMI = 0.45 DU (Fig. 10 Panel B). The percent difference plot shows that there is a
380 systematic increase between PANDORA and OMI TCNO₂ from a value 10% to a value of 50%.

381

382 **4.0 Summary**

383 Examination of long-term TCNO₂ monthly average time series from OMI satellite and PANDORA
384 ground-based observations show that OMI systematically underestimates the amount of NO₂ in the
385 atmosphere by an average factor of 1.5 to 2 at the local OMI overpass time near the equator crossing time
386 of 13:30±1:30. As shown in Fig. 7 for TCNO₂, $100(OMI - PAN)/PAN$ least squares mean underestimates are
387 much larger than error estimates. These differences are reduced for the smaller pixel size TropOMI TCNO₂
388 values (Judd et al., 2019). In addition, the PANDORA diurnal time series for every day during a year at each
389 site (only two typical sites are shown in this paper, NYC and NASA-HQ) shows peaks in TCNO₂ that are
390 completely missed by only observing at mid-day (see Figs. 6, 8, 9, and A2). The result is that estimates of
391 air quality related to health effects from OMI observations are strongly underestimated almost
392 everywhere as shown at all the sites with a long PANDORA record. In comparisons to PANDORA, OMI data
393 are mostly uncorrelated or weakly correlated (e.g., Seoul correlation coefficient $r^2 = 0.06$, Mauna Loa $r^2 =$
394 0.3), while NASA HQ in Washington, DC shows a correlation on a seasonal basis (NASA HQ $r^2 = 0.7$)
395 suggesting a wide area coordinated source of NO₂ (most likely automobile traffic). The data from CCNY
396 shows some correlation between the locations of the peaks and troughs. Seven short term TCNO₂ time
397 series were examined showing similar results (Table 1), except when the pollution region is widespread
398 as in the Seoul South Korea region. The conclusion is that while OMI satellite TCNO₂ data are uniquely
399 able to assess regional long-term trends in TCNO₂ and provide a measure of the regional distribution of
400 pollutants, the OMI data cannot properly assess local air quality or the effect on human health over
401 extended periods in urban or industrial areas. This will continue to be the case, but to a lesser degree,
402 when the OMI TCNO₂ data are improved by reprocessing with a new geometry-dependent reflectivity
403 (Vasilkov, 2017) and by the smaller FOV of TropOMI. The analysis shows that locating PANDORAs at
404 polluted sites could provide quantitative corrections for spatial and temporal biases that affect the
405 determination of local air quality from satellite data. Satellite detection of diurnal variation of TCNO₂ will
406 be improved with the upcoming launch of three planned geostationary satellites over Korea, US, and

407 Europe To verify the proper operation of the various PANDORA instruments, a similar analysis for Total
 408 Column Ozone TCO was performed (see Appendix) and shows close agreement between OMI and
 409 PANDORA, with the largest difference occurring for Mauna Loa Observatory at 3.4 km altitude, where
 410 PANDORA misses the ozone between the surface and 3.4 km.

411 **Appendix**

412 **Ozone:** This section shows the corresponding PANDORA total column ozone (TCO) values
 413 compared to OMI TCO for Busan South Korea (Fig. A1) that shows close agreement for the entire 2012 –
 414 2017 period. The different fields of view for OMI and PANDORA have a much smaller effect because of
 415 the greater spatial uniformity of stratospheric ozone compared to tropospheric NO₂. Additional sites are
 416 summarized in Table A1. The largest TCO difference (15 DU or 5.6%) occurs for Mauna Loa Observatory
 417 (Altitude = 3.4 km) compared to OMI (Average altitude = Sea Level). The close results show that the
 418 PANDORA was working properly and pointing accurately at the sun. The PANDORA TCO data shown here
 419 use a mid-latitude effective ozone temperature correction from model calculations that may not be
 420 accurate of each individual site (Herman et al., 2017). The ozone retrievals shown here use an average
 421 effective ozone temperature instead of a locally measured ozone temperature (Herman et al.,
 422 2015;2017).

423

424

Table A1 Average values of TCO₃ for PANDORA and OMI

Location	PAN (DU)	OMI (DU)	Percent Difference
Mauna Loa Observatory Hawaii (3.394 km)*	254	269	5.6
NASA HQ Washington DC (0.02 km)	308	314	1.9
Waterflow New Mexico (1.64 km)	293	292	0.3
Yonsei University Seoul South Korea (0.07 km)	317	325	2.5
Busan University Busan South Korea(0.03 km)	313	315	0.6
Boulder, Colorado (NOAA Bldg) (1.617 km)	299	302	1.0
Buenos Aires, Argentina (0.025 km)	279	284	1.8
Essex, Maryland (0.012 km)	299	301	0.7
Baltimore, Maryland (0.01 km)	296	296	0.0
Fresno, California (0.939 km)	306	309	1.0
Denver La Casa Colorado (1.6 km)	292	294	0.7
Gwangju Institute of Science and Technology (GIST) S. Korea (0.021 km)	302	307	1.6
Hankuk University Foreign Studies (HUFS) South Korea (0.04 km)	318	326	2.5
City College Manhattan New York City (0.04 km)	316	325	2.8
Average	299	304	1.6

425

426 **Mauna Loa TCNO₂:** Figure A2 shows the diurnal variation of TCNO₂ at MLO on specific days
 427 3,4,7, and 8 of June 2016 along with the variation in SZA. This shows that the MLO is polluted by NO₂

428 with column amounts in excess of stratospheric amounts (approximately 0.1 DU) even though there are
429 no local sources. OMI retrievals of TCNO₂ on each day are much lower (about 0.12 DU) because of the
430 averaging over OMI's large FOV that includes very clean ocean areas.

431

432

433

434

435

436

437 **Acknowledgement:** This project is supported by the Korea Ministry of Environment (MOE) as Public Technology
438 Program based on Environmental Policy (2017000160001), by the Los Alamos National Laboratory's Laboratory
439 Directed Research and Development program and by the NASA Pandora project managed by Dr. Robert
440 Swap.

441 **References**

442

443 Almaraz, Maya, Edith Bai, Chao Wang, Justin Troussel, Stephen Conley, Ian Faloon and Benjamin Z.
444 Houlton, Agriculture is a major source of NO_x pollution in California, *SCIENCE ADVANCES*, 31,
445 DOI:10.1126/sciadv.aao3477, 2018.

446

447 Amin, Md. Shohel Reza, Umma Tamima, and Luis Amador Jimenez, "Understanding Air Pollution from
448 Induced Traffic during and after the Construction of a New Highway: Case Study of Highway 25 in
449 Montreal," *Journal of Advanced Transportation*, vol. 2017, Article ID 5161308, 14 pages,
450 2017. <https://doi.org/10.1155/2017/5161308>, 2017.

451

452 Andersen, M. Hvidberg, S.S. Jensen, M. Ketzel, S. Loft, M. Sørensen, A. Tjønneland, K. Overvad, O. Raaschou-Nielsen
453 Chronic obstructive pulmonary disease and long-term exposure to traffic-related air
454 pollution: A cohort study, *Am. J. Respir. Crit. Care Med.*, 183, pp. 455-461, [10.1164/rccm.201006-0937OC](https://doi.org/10.1164/rccm.201006-0937OC), 2011.

456 Bechle, M. J.; Millet, D. B.; Marshall, J. D. Remote sensing of exposure to NO₂: Satellite versus ground-
457 based measurement in a large urban area. *Atmos. Environ.*, 69, 345-353, 2013

458

459 Bishop, Gary A. and Donald H. Stedman, Reactive Nitrogen Species Emission Trends in Three Light-
460 /Medium-Duty United States Fleets, *Environmental Science & Technology* 2015 49 (18), 11234-11240,
461 DOI: 10.1021/acs.est.5b02392, 2015.

462

463 Boersma, K. F., H. J. Eskes, E. J. Brinksma, Error analysis for tropospheric NO₂ retrieval from space, *J.*
464 *Geophys. Res. Atmos.*, <https://doi.org/10.1029/2003JD003962>, 2004.

465 Boersma, K. F., Eskes, H. J., Dirksen, R. J., van der A, R. J., Veefkind, J. P., Stammes, P., Huijnen, V.,
466 Kleipool, Q. L., Sneep, M., Claas, J., Leitão, J., Richter, A., Zhou, Y., and Brunner, D.: An improved
467 tropospheric NO₂ column retrieval algorithm for the Ozone Monitoring Instrument, *Atmos. Meas. Tech.*,
468 4, 1905-1928, <https://doi.org/10.5194/amt-4-1905-2011>, 2011.

469 Boersma, K. F., Vinken, G. C. M., & Eskes, H. J., Representativeness errors in comparing chemistry
470 transport and chemistry climate models with satellite UV-Vis tropospheric column retrievals.
471 *Geoscientific Model Development*, 9(2), 875-898, 2016.

472 Choudhari, Sheetal Korde, Minal Chaudhary, Sachin Bagde, Amol R Gadbai and Vaishali Joshi, Nitric oxide
473 and cancer: a review, *World Journal of Surgical Oncology* 2013, 11:118,
474 <http://www.wjso.com/content/11/1/118>, 2013.

475

476 Cleveland, William S., *LOWESS: A program for smoothing scatterplots by robust locally weighted*
477 *regression. The American Statistician*. 35 (1): 54. [JSTOR 2683591](https://doi.org/10.2307/2683591). [doi:10.2307/2683591](https://doi.org/10.2307/2683591), 1981.

478

479

480 Dirksen, Ruud J., K. Folkert Boersma, Henk J. Eskes, Dmitry V. Ionov, Eric J. Bucsela, Pieternel F. Levelt,
481 Hennie M. Kelder, Evaluation of stratospheric NO₂ retrieved from the Ozone Monitoring Instrument:
482 Intercomparison, diurnal cycle, and trending, *J. Geophys. Res.*, 116,
483 <https://doi.org/10.1029/2010JD014943>, 2011.

484

485 Duncan, B. N., L. N. Lamsal, A. M. Thompson, Y. Yoshida, Z. Lu, D. G. Streets, M. M. Hurwitz, and K. E.
486 Pickering, A space-based, high-resolution view of notable changes in urban NO_x pollution around the
487 world (2005–2014), *J. Geophys. Res. Atmos.*, 121, 976–996, doi:10.1002/2015JD024121, 2016.

488

489 Goldberg, D. L., Saide, P. E., Lamsal, L. N., de Foy, B., Lu, Z., Woo, J.-H., Kim, Y., Kim, J., Gao, M., Carmichael,
490 G., and Streets, D. G.: A top-down assessment using OMI NO₂ suggests an underestimate in the NO_x
491 emissions inventory in Seoul, South Korea during KORUS-AQ, *Atmos. Chem. Phys. Discuss.*,
492 <https://doi.org/10.5194/acp-2018-678>, in review, 2018.

493

494 Harkey, M., Holloway, T., Oberman, J., and Scotty, E., An evaluation of CMAQ NO₂ using observed
495 chemistry-meteorology correlations, *J. Geophys. Res. Atmos.*, 120, 11,775– 11,797,
496 doi:10.1002/2015JD023316, 2015.

497

498 Herman, J., A. Cede, E. Spinei, G. Mount, M. Tzortziou, and N. Abuhassan, NO₂ column amounts from
499 ground-based Pandora and MFDOAS spectrometers using the direct-sun DOAS technique:
500 Intercomparisons and application to OMI validation, *J. Geophys. Res.*, 114, D13307,
501 doi:10.1029/2009JD011848, 2009.

502

503 Herman, J.R., R.D. Evans, A. Cede, N.K. Abuhassan, I. Petropavlovskikh, and G. McConville, Comparison
504 of Ozone Retrievals from the Pandora Spectrometer System and Dobson Spectrophotometer in Boulder
505 Colorado, *Atmos. Meas. Tech.*, 8, 3407–3418, 2015 doi:10.5194/amt-8-3407-2015.

506

507 Herman, J., Evans, R., Cede, A., Abuhassan, N., Petropavlovskikh, I., McConville, G., Miyagawa, K., and
508 Noiro, B.: Ozone comparison between Pandora #34, Dobson #061, OMI, and OMPS in Boulder,
509 Colorado, for the period December 2013–December 2016, *Atmos. Meas. Tech.*, 10, 3539–3545,
510 <https://doi.org/10.5194/amt-10-3539-2017>, 2017.

511

512 Herman, J., Spinei, E., Fried, A., Kim, J., Kim, J., Kim, W., Cede, A., Abuhassan, N., and Segal-Rozenhaimer,
513 M.: NO₂ and HCHO measurements in Korea from 2012 to 2016 from Pandora spectrometer instruments
514 compared with OMI retrievals and with aircraft measurements during the KORUS-AQ campaign, *Atmos.*
515 *Meas. Tech.*, 11, 4583–4603, <https://doi.org/10.5194/amt-11-4583-2018>, 2018.

516

517 Ialongo, I., Herman, J., Krotkov, N., Lamsal, L., Boersma, K. F., Hovila, J., and Tamminen, J.: Comparison of
518 OMI NO₂ observations and their seasonal and weekly cycles with ground-based measurements in Helsinki,
519 *Atmos. Meas. Tech.*, 9, 5203–5212, <https://doi.org/10.5194/amt-9-5203-2016>, 2016.

520

521 Judd, Laura M., Jassim A. Al-Saadi, Lukas C. Valin, R. Bradley Pierce, Kai Yang, Scott J. Janz, Matthew G.
522 Kowalewski, James J. Szykman, Martin Tiefengraber, and Moritz Mueller, The Dawn of Geostationary Air

523 Quality Monitoring: Case Studies From Seoul and Los Angeles, Environ.
524 Sci.,<https://doi.org/10.3389/fenvs.2018.00085>, 2018.
525
526 Judd, L. M., Al-Saadi, J. A., Janz, S. J., Kowalewski, M. G., Pierce, R. B., Szykman, J. J., Valin, L. C., Swap, R.,
527 Cede, A., Mueller, M., Tiefengraber, M., Abuhassan, N., and Williams, D.: Evaluating the impact of spatial
528 resolution on tropospheric NO₂ column comparisons within urban areas using high-resolution airborne
529 data, Atmos. Meas. Tech. Discuss., <https://doi.org/10.5194/amt-2019-161>, in review, 2019.
530
531 Kleipool, Q.L., M.R. Dobber, J.F. De Haan and P.F. Levelt, Earth Surface Reflectance Climatology from Three
532 Years of OMI Data, Journal of Geophysical Research, 113, doi:10.1029/2008JD010290, 2008.
533
534 Knepp, T., M. Pippin, J. Crawford, Jim Szykman, R. Long, L. Cowen, A. Cede, N. Abuhassan, J. Herman, R.
535 Delgado, J. Compton, T. Berkoff, J. Fishman, D. Martins, R. Stauffer, A. Thompson, A. Weinheimer, D.
536 Knapp, D. Montzka, D. Lenschow, AND D. Neil. Estimating Surface NO₂ and SO₂ Mixing Ratios from Fast-
537 Response Total Column Observations and Potential Application to Geostationary Missions. JOURNAL OF
538 ATMOSPHERIC CHEMISTRY. Springer, New York, NY, 0(0):1-26, (2014).
539
540 Kollonige, D. E., Thompson, A. M., Josipovic, M., Tzortziou, M., Beukes, J. P., Burger, R., ... Laakso, L. (2018).
541 OMI satellite and ground-based Pandora observations and their application to surface NO₂ estimations
542 at terrestrial and marine sites. Journal of Geophysical Research: Atmospheres, 123, 1441–1459.
543 <https://doi.org/10.1002/2017JD026518>, 2018.
544
545 Krotkov, N. A., Lamsal, L. N., Celarier, E. A., Swartz, W. H., Marchenko, S. V., Bucsela, E. J., Chan, K. L.,
546 Wenig, M., and Zara, M.: The version 3 OMI NO₂ standard product, Atmos. Meas. Tech., 10, 3133-3149,
547 <https://doi.org/10.5194/amt-10-3133-2017>, 2017.
548
549 Lamsal, L & Martin, Randall & Parrish, David & Krotkov, Nickolay., Scaling Relationship for NO₂ Pollution
550 and Urban Population Size: A Satellite Perspective. Environmental science & technology. 47.
551 10.1021/es400744g, 2013.
552
553 Lamsal, L. N., Krotkov, N. A., Celarier, E. A., Swartz, W. H., Pickering, K. E., Bucsela, E. J., Martin, R.
554 V., Philip, S., Irie, H., Cede, A., Herman, J., Weinheimer, A., Szykman, J. J., and Knepp, T. N.: Evaluation
555 of OMI operational standard NO₂ column retrievals using in situ and surface-based NO₂ observations,
556 Atmos. Chem. Phys. Discuss., 14, 14519-14573, doi:10.5194/acpd-14-14519-2014, 2014.
557
558 Lamsal, L. N., S. J. Janz, N. A. Krotkov, K. E. Pickering, R. J. D. Spurr, M. G. Kowalewski, C. P. Loughner, J. H.
559 Crawford, W. H. Swartz, and J. R. Herman, High-resolution NO₂ observations from the Airborne Compact
560 Atmospheric Mapper Retrieval and validation, J. Geophys. Res. Atmos., 122, 1953–1970,
561 doi:10.1002/2016JD025483, 2017
562

563 Levelt, P. F., Van den Oord, G. H. J., Dobber, M. R., Malkki, A., Visser, H., de Vries, J., Stammes, P., Lundell,
564 J. O. V., and Saari, H.: The Ozone Monitoring Instrument, *IEEE T. Geosci. Remote*, 44, 1093–1101,
565 doi:10.1109/tgrs.2006.872333, 2006.

566

567 Lindenmaier, Rodica, Manvendra K. Dubey, Bradley G. Henderson, Zachary T. Butterfield, Jay R. Herman,
568 Thom Rahn · S.-H. Lee, Multiscale observations of CO₂, (CO₂)-C-13, and pollutants at Four Corners for
569 emission verification and attribution, *Proceedings of the National Academy of Sciences* 06/2014;
570 111(23):8386-8391. DOI:10.1073/pnas.132188311, 2014

571

572 Liu, F., Beirle, S., Zhang, Q., Dörner, S., He, K., and Wagner, T.: NO_x lifetimes and emissions of cities and
573 power plants in polluted background estimated by satellite observations, *Atmos. Chem. Phys.*, 16, 5283-
574 5298, <https://doi.org/10.5194/acp-16-5283-2016>, 2016.

575

576 Lorente, A., Boersma, K. F., Stammes, P., Tilstra, L. G., Richter, A., Yu, H., Kharbouche, S., and Muller, J.-P.:
577 The importance of surface reflectance anisotropy for cloud and NO₂ retrievals from GOME-2 and OMI,
578 *Atmos. Meas. Tech.*, 11, 4509-4529, <https://doi.org/10.5194/amt-11-4509-2018>, 2018.

579

580 Nowlan, C. R., Liu, X., Leitch, J. W., Chance, K., González Abad, G., Liu, C., Zoogman, P., Cole, J., Delker, T.,
581 Good, W., Murcray, F., Ruppert, L., Soo, D., Follette-Cook, M. B., Janz, S. J., Kowalewski, M. G., Loughner,
582 C. P., Pickering, K. E., Herman, J. R., Beaver, M. R., Long, R. W., Szykman, J. J., Judd, L. M., Kelley, P., Luke,
583 W. T., Ren, X., and Al-Saadi, J. A.: Nitrogen dioxide observations from the Geostationary Trace gas and
584 Aerosol Sensor Optimization (GeoTASO) airborne instrument: Retrieval algorithm and measurements
585 during DISCOVER-AQ Texas 2013, *Atmos. Meas. Tech.*, 9, 2647-2668, [https://doi.org/10.5194/amt-9-](https://doi.org/10.5194/amt-9-2647-2016)
586 2647-2016, 2016.

587

588 O’Byrne, G., R. V. Martin, A. van Donkelaar, J. Joiner, and E. A. Celarier, Surface reflectivity from the Ozone
589 Monitoring Instrument using the Moderate Resolution Imaging Spectroradiometer to eliminate clouds:
590 Effects of snow on ultraviolet and visible trace gas retrievals, *J. Geophys. Res.*, VOL. 115, D17305,
591 doi:10.1029/2009JD013079, 2010.

592

593 Marchenko, S., N. A. Krotkov, L. N. Lamsal, E. A. Celarier, W. H. Swartz, and E. J. Bucsela, Revising the
594 slant column density retrieval of nitrogen dioxide observed by the Ozone Monitoring Instrument, *J.*
595 *Geophys. Res. Atmos.*, 120, 5670–5692, doi:10.1002/2014JD022913, 2015

596

597 Park, Se Hoon, Seoul, The Wiley Blackwell Encyclopedia of Urban and Regional Studies. Edited by
598 Anthony Orum. John Wiley & Sons Ltd. Published 2019 by John Wiley & Sons Ltd. DOI:
599 10.1002/9781118568446.eurs0283, 2019.

600

601 Raponi, Marcelo, Cede, A, Santana Diaz, Daniel, Sanchez, R, A. Otero, L, O. Salvador, J, R. Ristori, P, Quel,
602 Eduardo. Total Column Ozone Measured In Buenos Aires Between March And November 2017, Using A
603 Pandora Spectrometer System. *Anales AFA*. 29(2), 46-50. 10.31527/analesafa.2018.29.2.46, 2018.

604

605 Seo, J., Park, D.-S. R., Kim, J. Y., Youn, D., Lim, Y. B., and Kim, Y.: Effects of meteorology and
606 emissions on urban air quality: a quantitative statistical approach to long-term records (1999–2016)
607 in Seoul, South Korea, *Atmos. Chem. Phys.*, 18, 16121-16137, [https://doi.org/10.5194/acp-18-](https://doi.org/10.5194/acp-18-16121-2018)
608 16121-2018, 2018.

609 Torres, O., Bhartia, P. K., Jethva, H., and Ahn, C.: Impact of the ozone monitoring instrument row
610 anomaly on the long-term record of aerosol products, *Atmos. Meas. Tech.*, **11**, 2701-2715,
611 <https://doi.org/10.5194/amt-11-2701-2018>, 2018.
612

613 Tzortziou, M.; Parker, O.; Lamb, B.; Herman, J.R.; Lamsal, L.; Stauffer, R.; Abuhassan, N. Atmospheric
614 Trace Gas (NO₂ and O₃) Variability in South Korean Coastal Waters, and Implications for Remote
615 Sensing of Coastal Ocean Color Dynamics. *Remote Sens.*, **10**, 1587, ; doi:10.3390/rs10101587, 2018.
616

617 Vasilkov, A., Qin, W., Krotkov, N., Lamsal, L., Spurr, R., Haffner, D., Joiner, J., Yang, E.-S., and Marchenko,
618 S.: Accounting for the effects of surface BRDF on satellite cloud and trace-gas retrievals: a new approach
619 based on geometry-dependent Lambertian equivalent reflectivity applied to OMI algorithms, *Atmos.*
620 *Meas. Tech.*, **10**, 333-349, <https://doi.org/10.5194/amt-10-333-2017>, 2017.
621

622 Zara, M., Boersma, K. F., De Smedt, I., Richter, A., Peters, E., van Geffen, J. H. G. M., Beirle, S.,
623 Wagner, T., Van Roozendaal, M., Marchenko, S., Lamsal, L. N., and Eskes, H. J.: Improved slant column
624 density retrieval of nitrogen dioxide and formaldehyde for OMI and GOME-2A from QA4ECV:
625 intercomparison, uncertainty characterization, and trends, *Atmos. Meas. Tech.*, **11**, 4033-4058,
626 <https://doi.org/10.5194/amt-11-4033-2018>, 2018.
627

628 Zheng, G. J., Duan, F. K., Su, H., Ma, Y. L., Cheng, Y., Zheng, B., Zhang, Q., Huang, T., Kimoto, T., Chang,
629 D., Pöschl, U., Cheng, Y. F., and He, K. B.: Exploring the severe winter haze in Beijing: the impact of
630 synoptic weather, regional transport and heterogeneous reactions, *Atmos. Chem. Phys.*, **15**, 2969–
631 2983, <https://doi.org/10.5194/acp-15-2969-2015>, 2015.

632
633
634

635 **Figure Captions**

636 Fig 1 Diurnal variation of TCNO₂ measured at Pusan University in Busan South Korea

637 Fig. 2. Monthly average values of TCNO₂ for OMI and PANDORA at OMI overpass times

638 Fig. 3 Extended time series for Busan. Left Panel: individual matching PANDORA and OMI data
639 points for the overpass time \pm 6 minutes. Right Panel: monthly averages.

640 Fig. 4. PANDORA compared to OMI. Extended TCNO₂ overpass time series for Mauna Loa
641 Observatory, Hawaii, NASA Headquarters, Washington DC, and Waterflow, New Mexico.

642 Fig. 5. PANDORA compared to OMI. Extended TCNO₂ overpass time series for Seoul South Korea,
643 Boulder, Colorado, and Buenos Aires, Argentina (Raponi et al. 2018).

644 Fig.6 Diurnal variation of TCNO₂ on a single day 1) Two km north of Waterflow, NM near a
645 power plant, 2) On the roof of NASA Headquarters Washington, DC and 3) On the roof of a
646 building at CCNY City College of New York, New York City

647 Fig. 7 Percent differences between OMI and PANDORA. The slopes are the absolute change in the
648 percent difference. For example, the Boulder percent difference goes from -31% to -23% over 4 years.
649 The LS Means are least squares means with the corresponding error estimates

650 Fig. 8A TCNO₂ diurnal variation (DU) from January to June, NASA Headquarters Washington, DC
651 from January 2015 to June 2015. The approximate OMI overpass time near 13:30 hours is marked.

652 Fig. 8B TCNO₂ diurnal variation (DU) from July to December, NASA Headquarters Washington, DC from
653 July 2015 to December 2015. The approximate OMI overpass time near 13:30 hours is marked

654 Fig. 9A TCNO₂ diurnal variation (DU) at CCNY in New York City January to June 2018. The approximate
655 OMI overpass time near 13:30 hours is marked.

656 Fig. 9B TCNO₂ diurnal variation at CCNY in New York City July to December 2018. The peak near 5 DU
657 occurs on 13 July 2018 between 11:20 and 12:30 EST. The approximate OMI overpass time near 13:30
658 hours is marked.

659 Fig. 10 TCNO₂ overpass time series for CCNY in Manhattan, New York City. Panel A: OMI
660 overpass TCNO₂ (Black) compare with OMI (Red). Panel B: Monthly Lowess(0.08) fit to the daily
661 overpass data. Panel C: Percent difference $100(\text{OMI} - \text{PAN})/\text{PAN}$ calculated from the data in
662 Panel A

663 Fig. A1 Monthly average values of TCO for OMI and PANDORA at OMI overpass times for Busan South
664 Korea. Shaded area represents the KORUS-AQ campaign period.

665 Fig. A2. The diurnal variation of TCNO₂ at MLO on 4 days during June 2016 compared to OMI TCNO₂
666 (small square). Shaded areas represent high SZA conditions where the PANDORA retrievals are not
667 accurate.

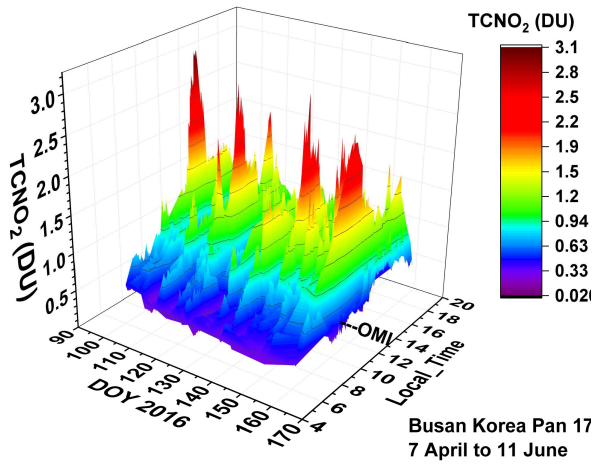


Fig 1 Diurnal variation of TCNO₂ measured at Pusan University in Busan South Korea

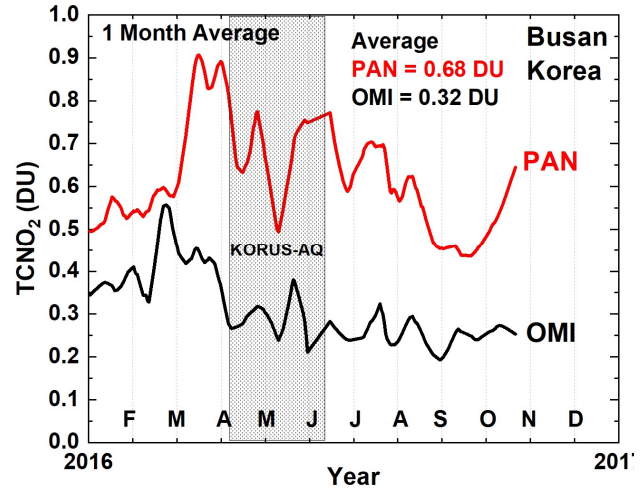


Fig. 2. Monthly average values of TCNO₂ for OMI and PANDORA at OMI overpass times

668

669

670

671 **FIGURE 1**

672

673

FIGURE 2

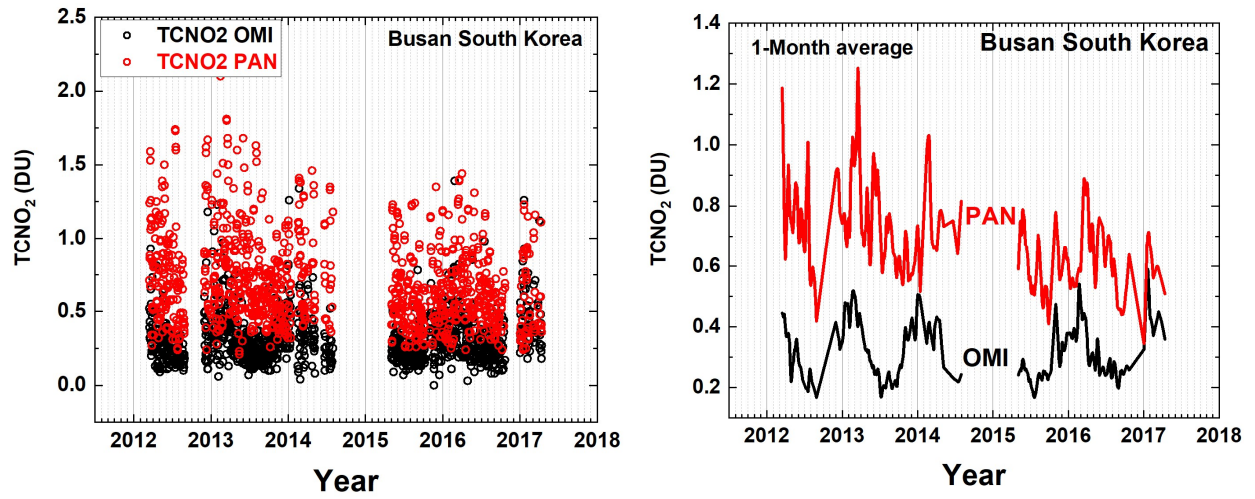


Fig. 3 Extended time series for Busan. Left Panel: individual matching PANDORA and OMI data points for the overpass time ± 6 minutes. Right Panel: monthly averages.

674

675

676 **FIGURE 3**

677

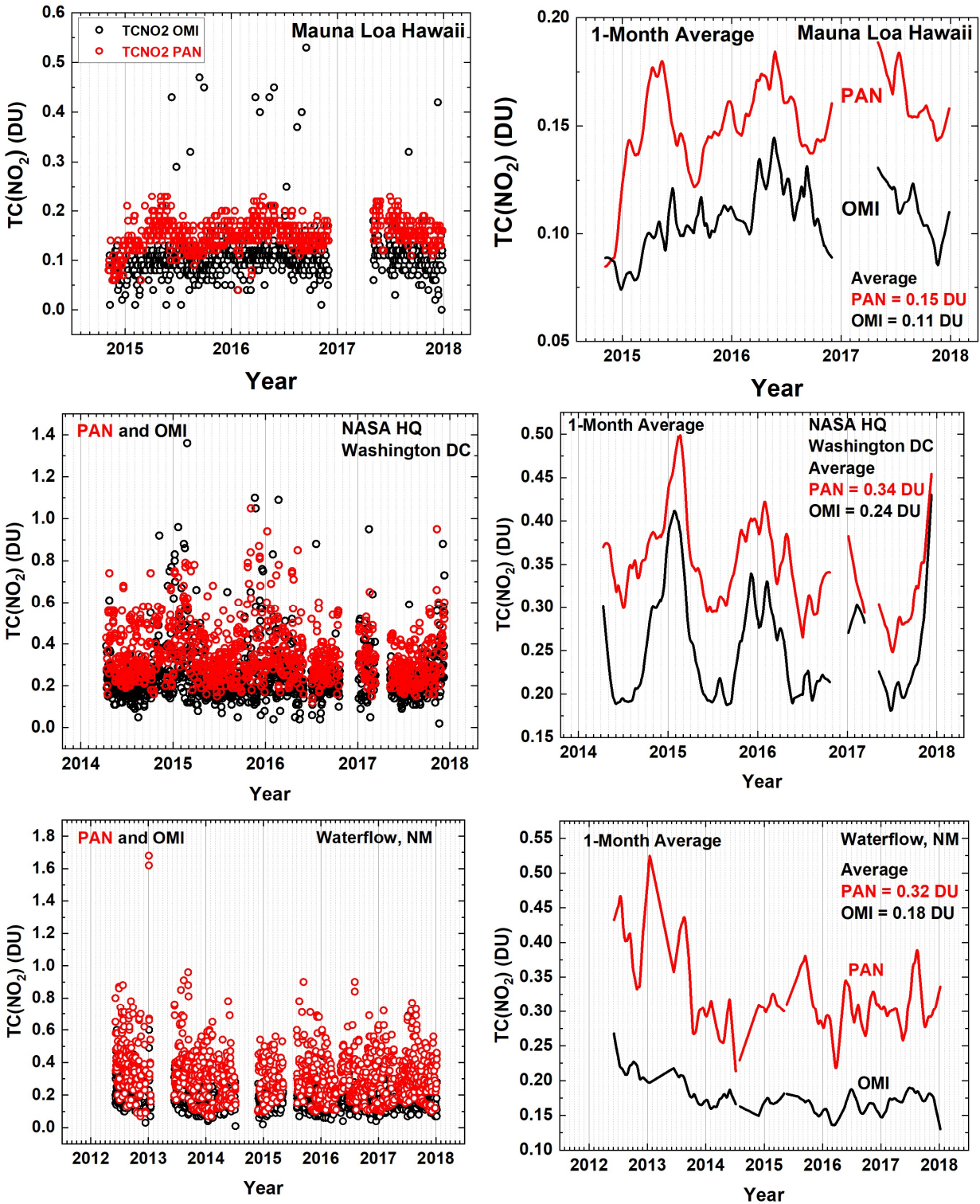


Fig. 4. PANDORA compared to OMI. Extended TCNO₂ overpass time series for Mauna Loa Observatory, Hawaii, NASA Headquarters, Washington DC, and Waterflow, New Mexico.

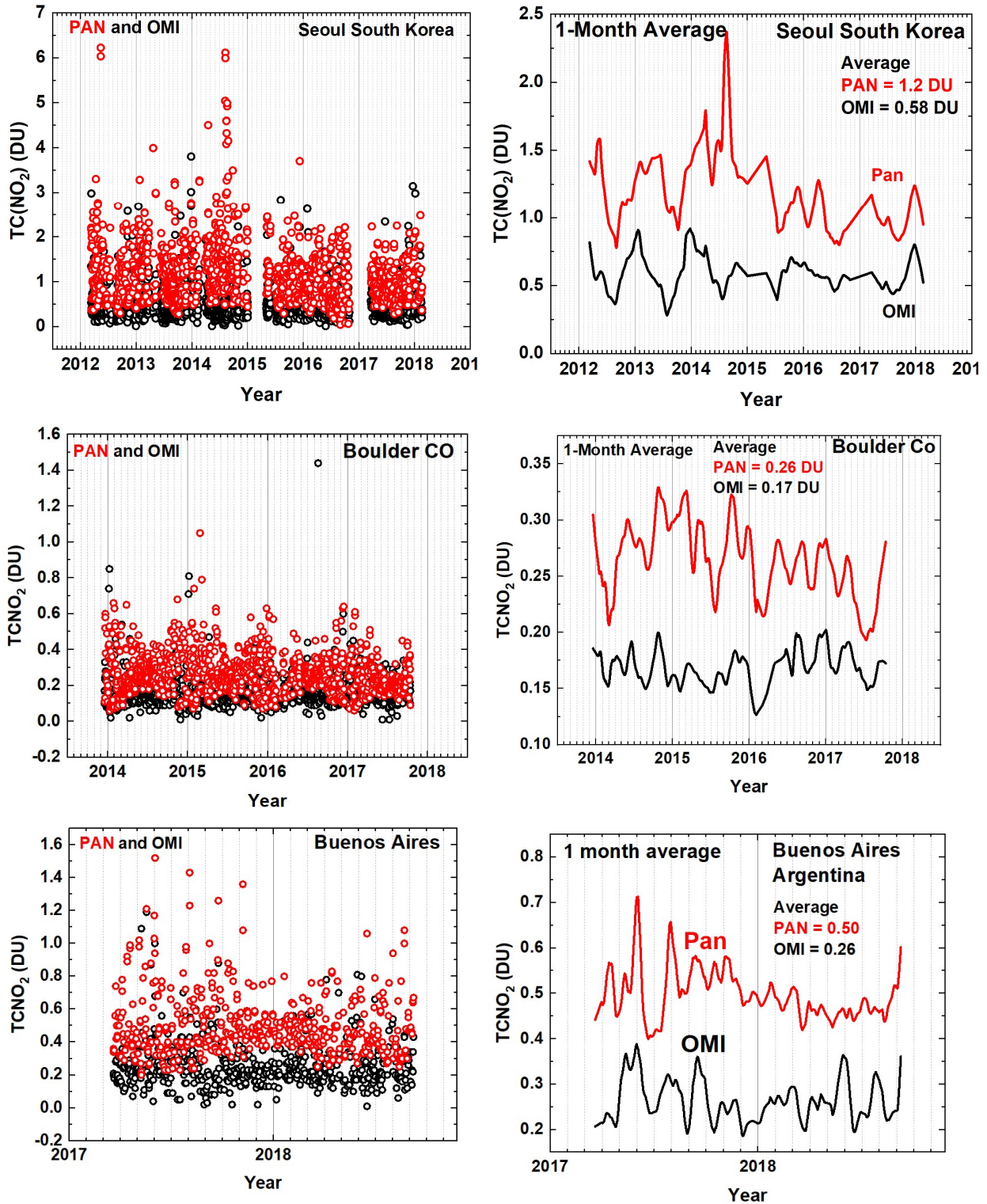


Fig. 5. PANDORA compared to OMI. Extended TCNO₂ overpass time series for Seoul South Korea, Boulder, Colorado, and Buenos Aires, Argentina (Raponi et al. 2017).

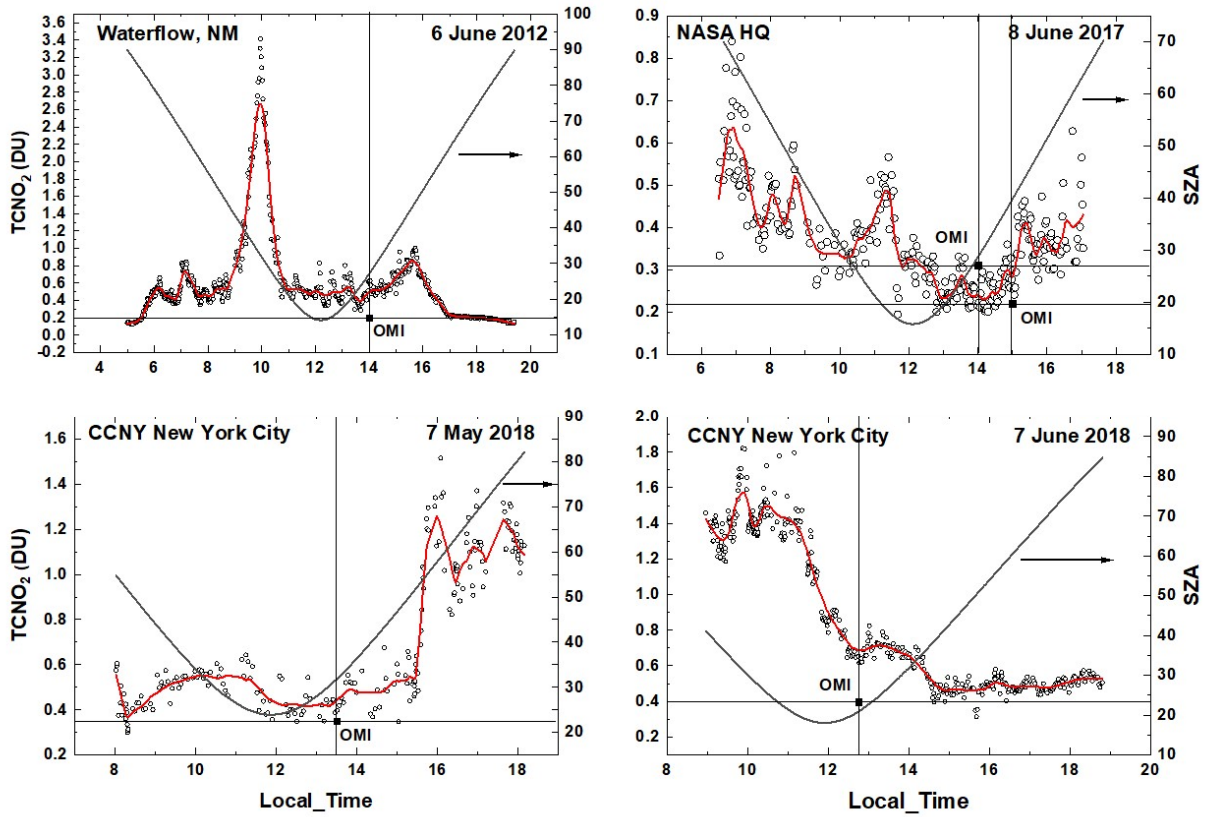


Fig.6 Diurnal variation of TCNO₂ on a single day 1) Two km north of Waterflow, NM near a power plant, 2) On the roof of NASA Headquarters Washington, DC and 3) On the roof or a building at City College of New York, New York City

680

681

682

683

684

685 **FIGURE 6**

686

687

688

689

690

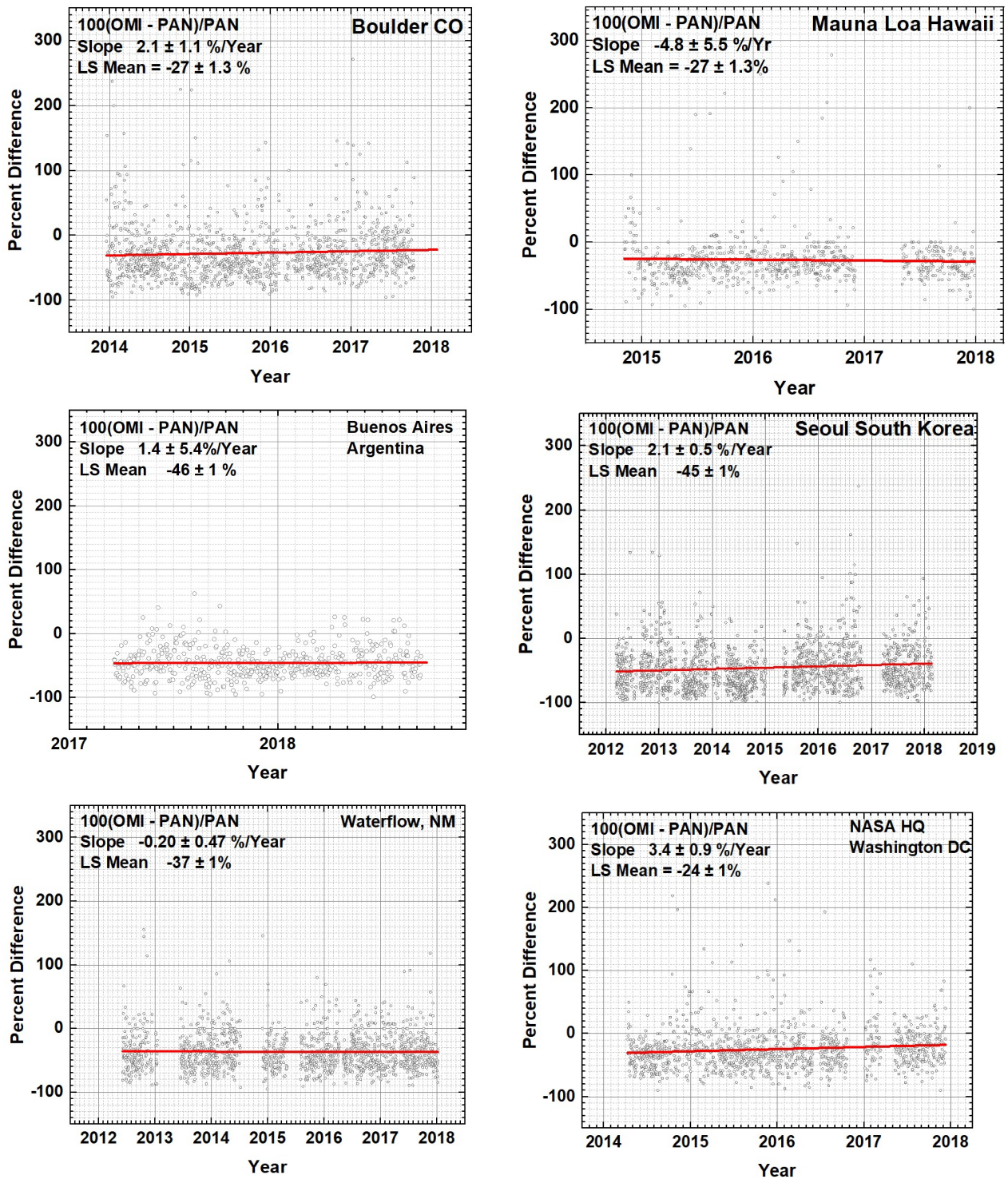


Fig. 7 Percent differences between OMI and PANDORA. The slopes are the absolute change in the percent difference. For example, the Boulder percent difference goes from -31% to -23% over 4 years. The LS Means are least squares means with the corresponding error estimates

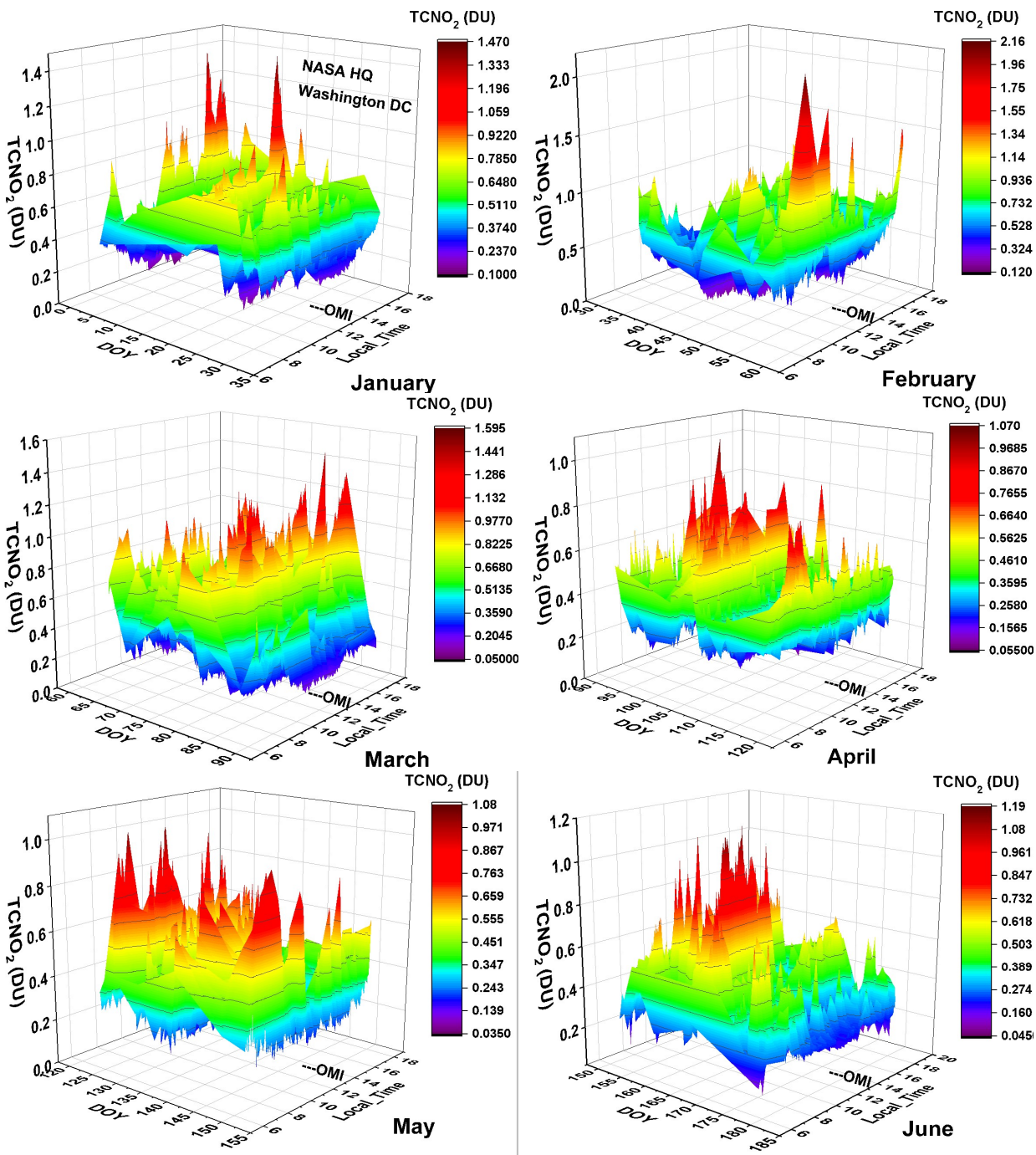


Fig. 8A TCNO₂ diurnal variation (DU) from January to June, NASA Headquarters Washington, DC from January 2015 to June 2015. The approximate OMI overpass time near 13:30 hours is marked

FIGURE 8A

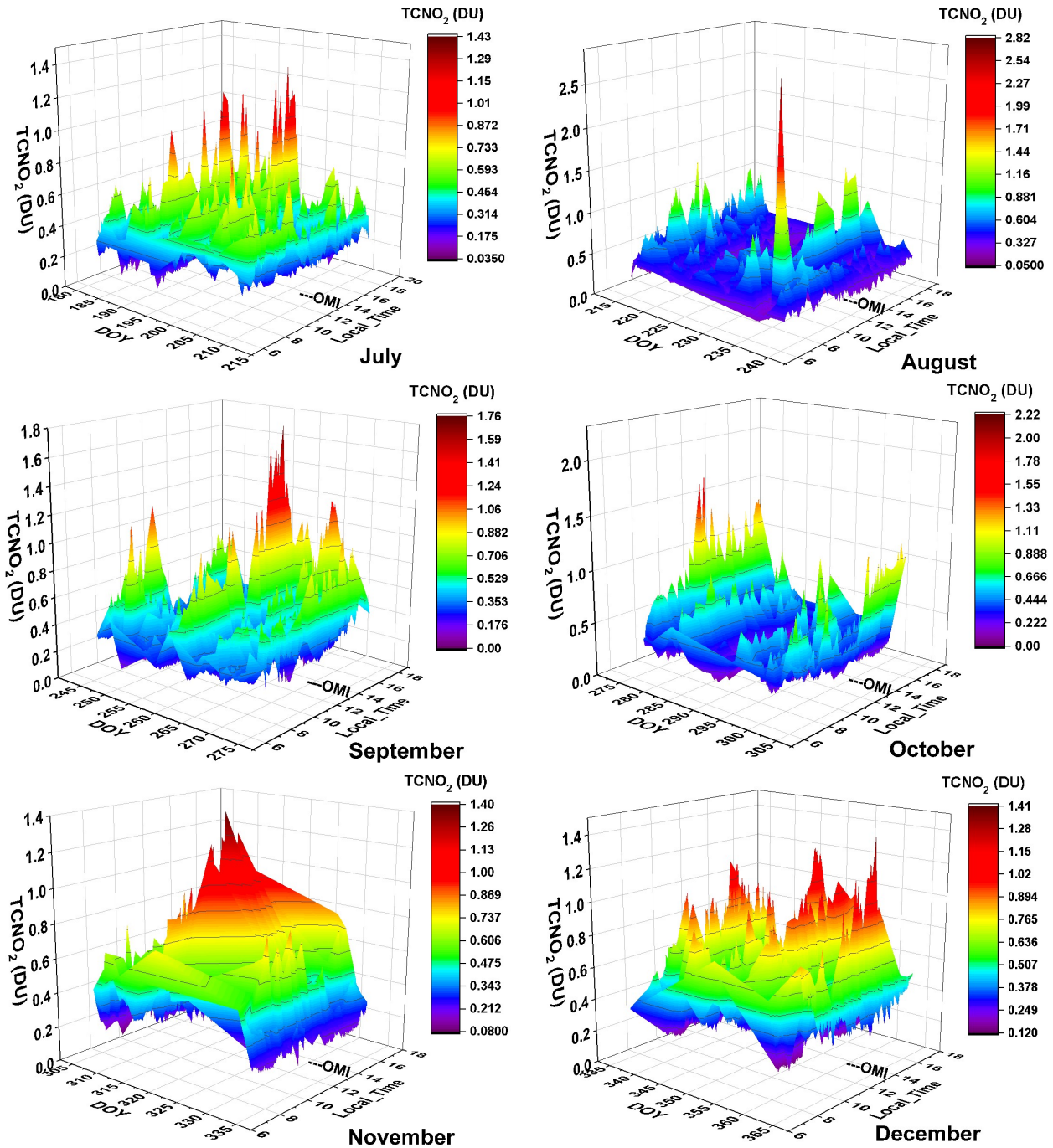


Fig. 8B TCNO₂ diurnal variation (DU) from July to December, NASA Headquarters Washington, DC from July 2015 to December 2015. The approximate OMI overpass time near 13:30 hours is marked.

693

694 **FIGURE 8B**

695

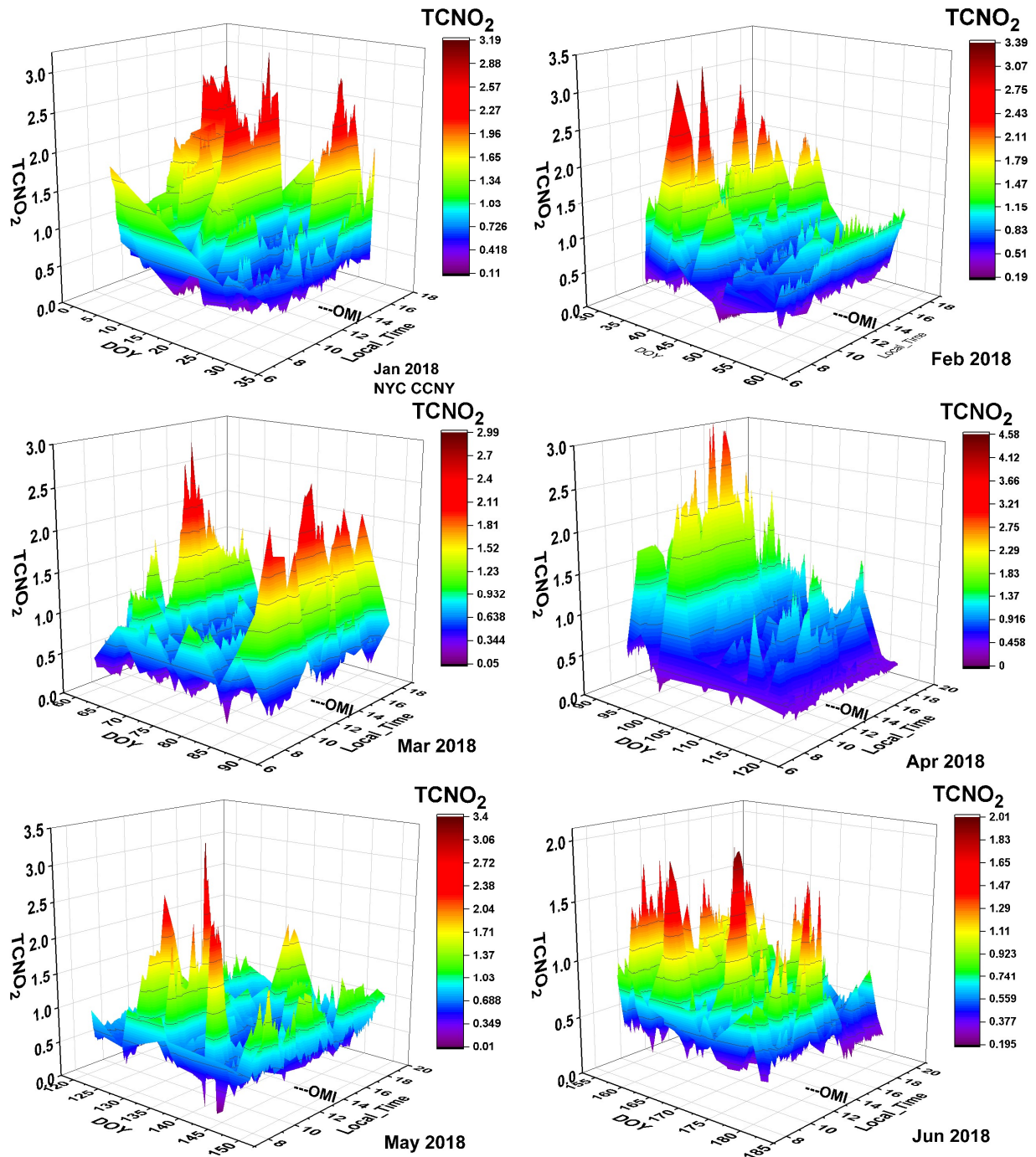


Fig. 9A TCNO₂ diurnal variation (DU) at CCNY in New York City January to June 2018. The approximate OMI overpass time near 13:30 hours is marked

696

697 **Figure 9A**

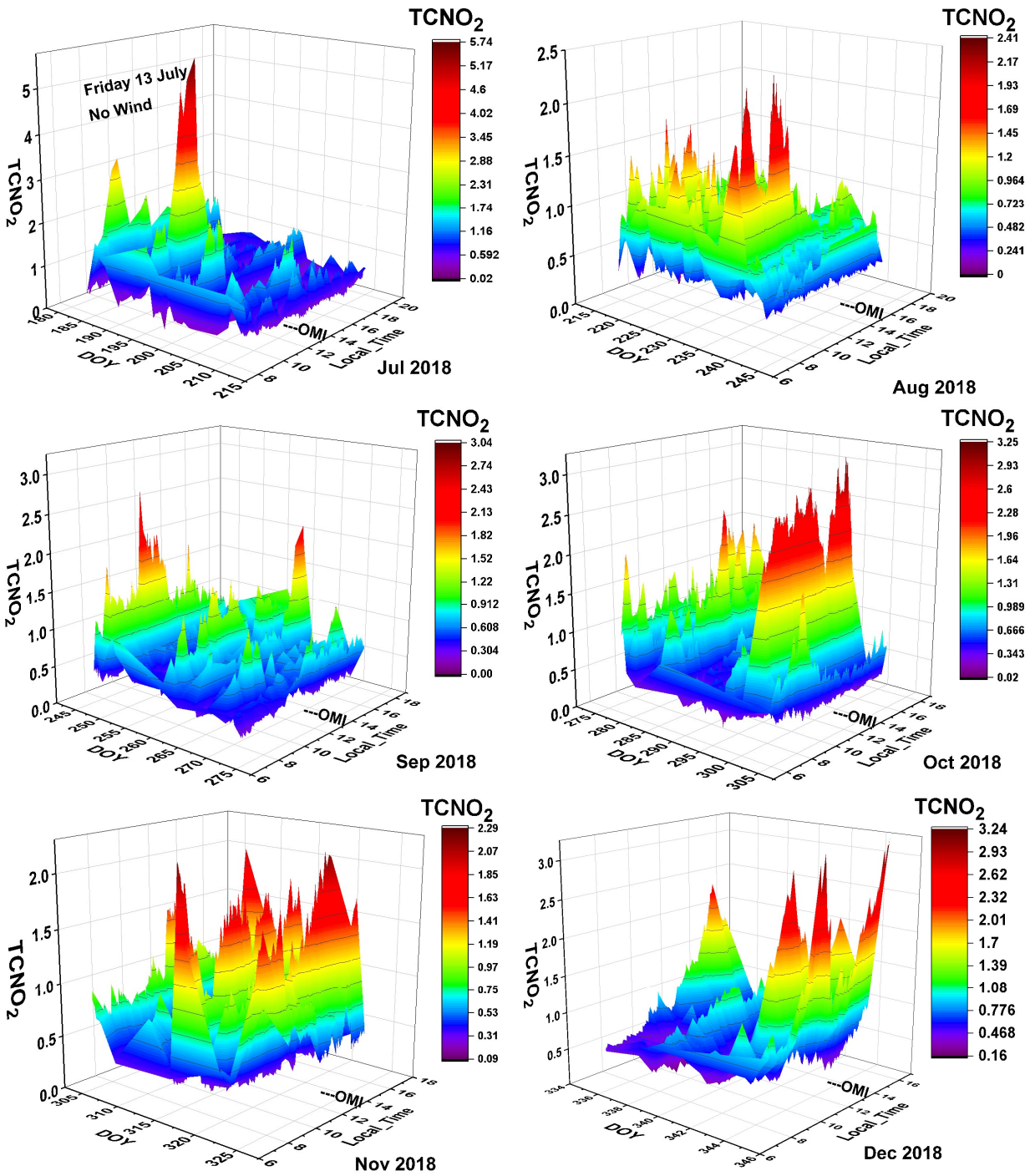


Fig. 9B TCNO₂ diurnal variation (DU) at CCNY in New York City July to December 2018. The peak near 5 DU occurs on 13 July 2018 between 11:20 and 12:30 EST. The approximate OMI overpass time near 13:30 hours is marked.

698

699 **Figure 9B**

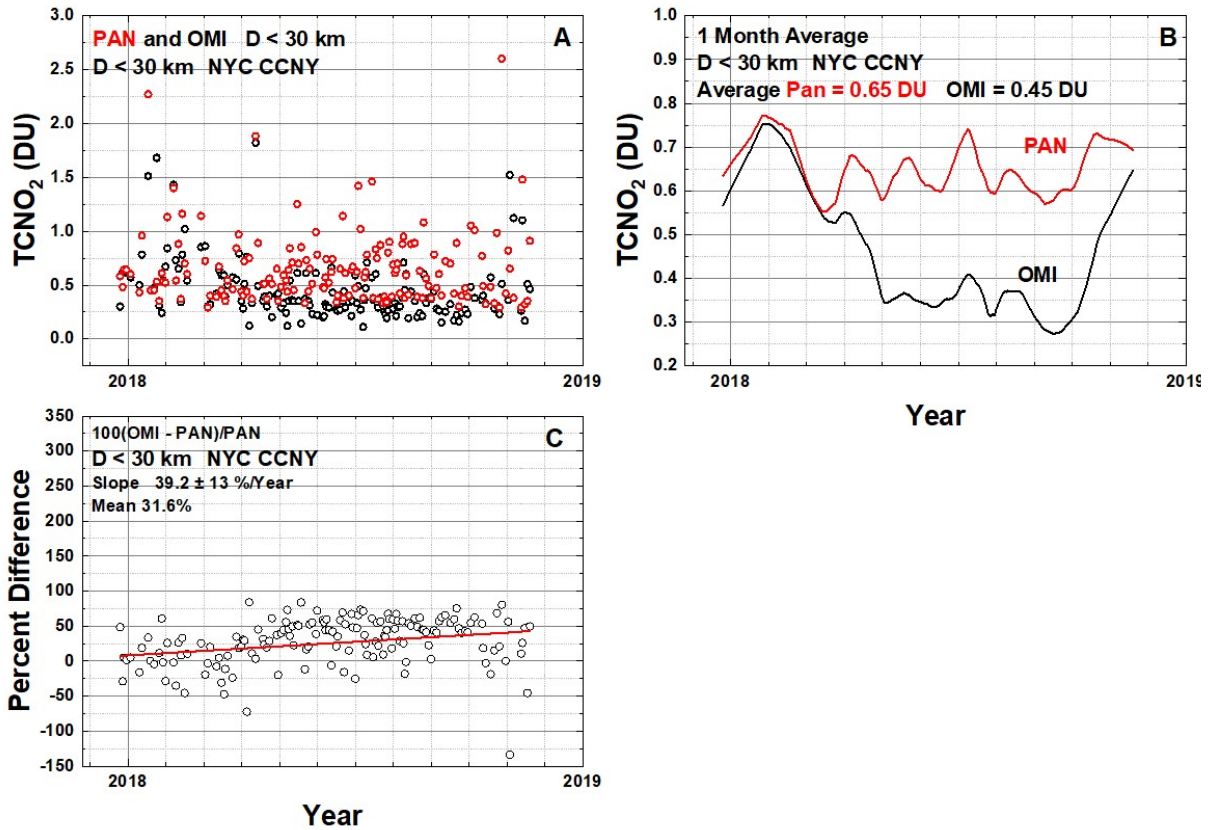


Fig. 10 TCNO₂ overpass time series for CCNY in Manhattan, New York City. OMI pixels are at a distance D < 30 km from CCNY. Panel A: OMI overpass TCNO₂ (Black) compare with OMI (Red). Panel B: Monthly Lowess(f) fit to the daily overpass data. Panel C: Percent difference $100(OMI - PAN)/PAN$ calculated from the data in Panel A

700

701 **Figure 10**

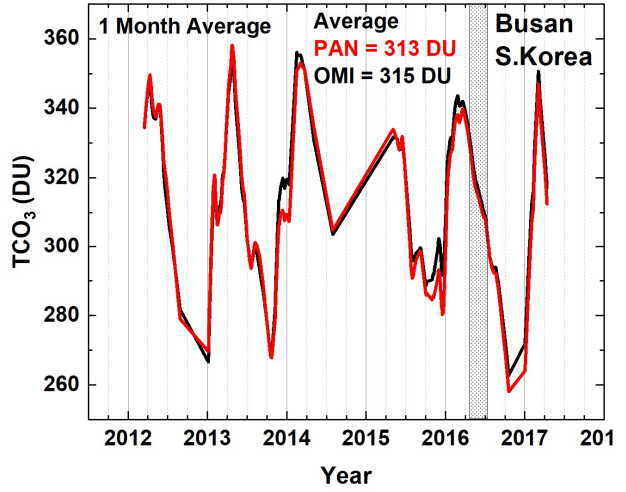
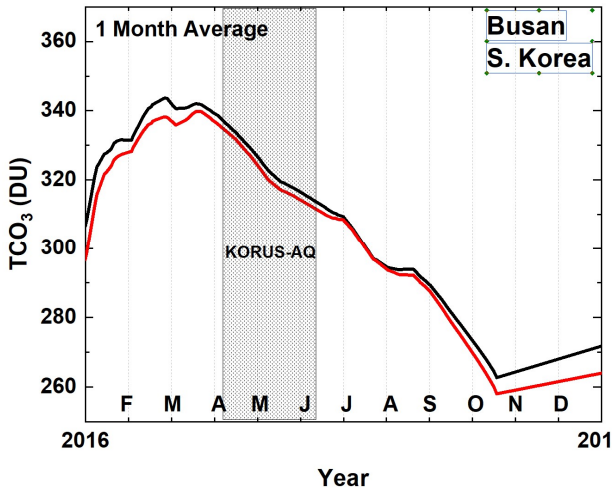


Fig. A1 Monthly average values of TCO_3 for OMI and PANDORA at OMI overpass times for Busan South Korea. Shaded area represents the KORUS-AQ campaign period.

702

703

704 **FIGURE A1**

705

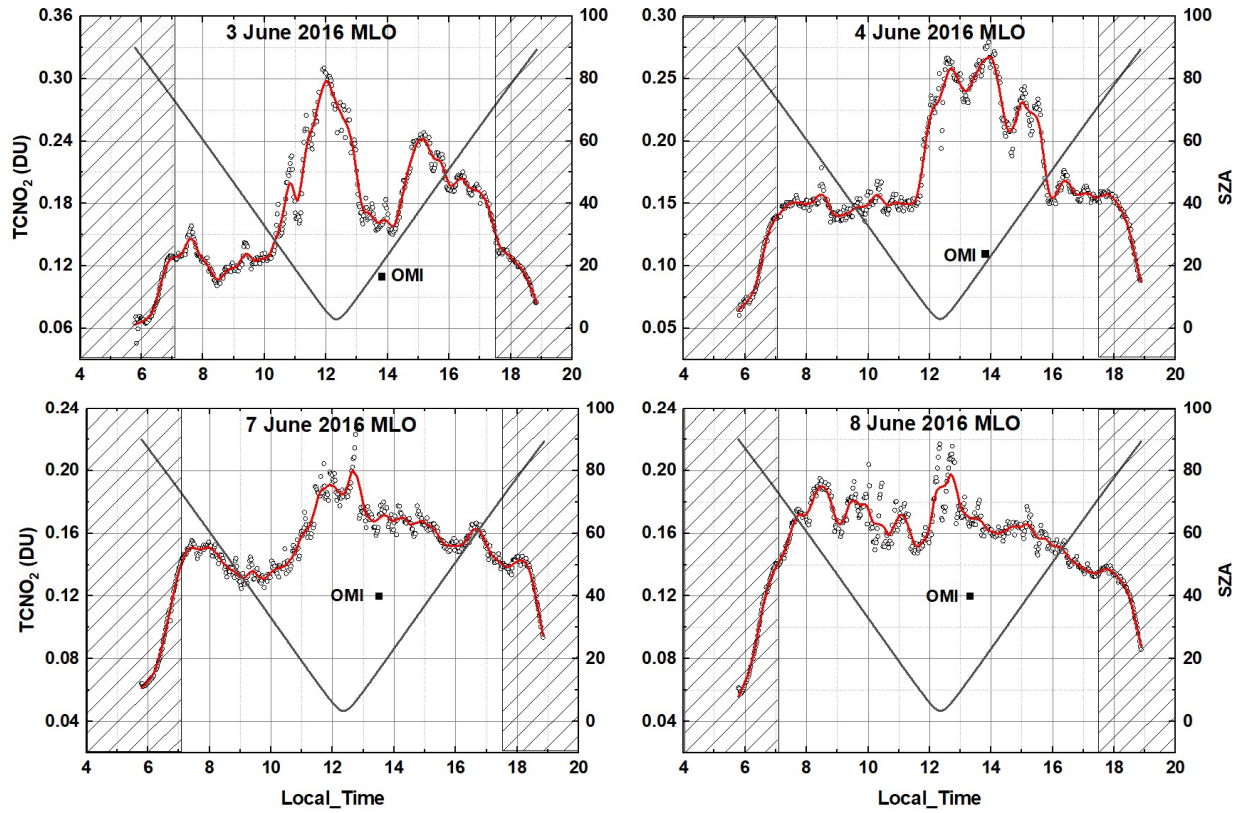


Fig. A2. The diurnal variation of TCNO₂ at MLO on 4 days during June 2016 compared to OMI TCNO₂ (small square). Shaded areas represent high SZA conditions where the PANDORA retrievals are not accurate.

706

707

708

709

710

711

712 **FIGURE A2**

713

714 **Author Contributions:** Jay Herman produced all of the figures and text, Jhoon and Jae Kim contributed
715 the Korean PANDORA data, Manvendra Dubey contributed the data from Waterflow, New Mexico and
716 the CO₂ analysis, Marcel Raponi contributed the Buenos Aires PANDORA data, And Maria Tzortziou
717 contributed the PANDORA data from CCNY.

718